Chapter 4
Kinetic theory models

Chinesta, Francisco ; Abisset-Chavanne Emmanuelle

Discrete techniques (MD or BD), despite their conceptual simplicity, are very often too expensive from the computational point of view. Kinetic theory approaches seems in many cases a suitable compromise between the accuracy of finer descriptions and the computational efficiency of macroscopic descriptions.

In this chapter we revisit some kinetic theory models. Even if there is a common rationale for deriving the different models, in order to emphasize their physical contents, we are following a diversity of alternative routes to derive them.

4.1 Motivation

As indicated above the atomistic description involves too rich kinematics. The atoms are vibrating (due to thermal effects) and small particles exhibit an erratic path due to the continuous impacts that they are enduring. Of course, appropriate averages of physical interest are most of the time governed by classical deterministic equations.

In the book written by Erwin Schrödinger untitled *What is the life? The physical aspects of the living cells* [46], the author states that the sensorial structures of the living beings need a multi-atomic structure to be protected from any random monoatomic event. A living being needs "exact" physical laws and for this reason our sensorial devices must filter the high frequency information (characteristic of the atomic behaviors) retaining only averages that evolve with a certain regularity. To perform this filtering process one needs multiatomic sensorial organs, as found in the vast majority of the living beings! In this way knowledge becomes simple and fast.

Kinetic theory losses individuality in favor of corser population descriptions. The kinetic theory framework will be described in this chapter by focusing on different physics.

4.2 Kinetic theory description of simple liquids and gases

In kinetic theory approaches we are interested in averages and not in individual behaviors anymore. Let N be a population of particles having an electrical charge. The system could be described by giving the position and velocity of each particle in the population at any time as it is the case in particles-based approaches. However this description is too expensive when we are only interested in averages and not in local effects as for example defaults propagation. In this way, we could introduce a distribution function giving the fraction of particles that at time t are located in a neighborhood of point $\mathbf{x}$ ($\mathbf{x} \in \mathbb{R}^3$) and having a velocity close to $\mathbf{v}$ ($\mathbf{v} \in \mathbb{R}^3$).

Thus, $\Psi(\mathbf{x},\mathbf{v},t)d\mathbf{x}d\mathbf{v}$ represents the fraction of those particles located inside the hexahedron $[x-\frac{dx}{2},x-\frac{dx}{2}]\times[y-\frac{dy}{2},y-\frac{dy}{2}]\times[z-\frac{dz}{2},z-\frac{dz}{2}]$ whose velocity is also inside the hexahedron $[u-\frac{du}{2},u-\frac{du}{2}]\times[v-\frac{dv}{2},v-\frac{dv}{2}]\times[\omega-\frac{d\omega}{2},\omega-\frac{d\omega}{2}]$, where the components of the position and velocity vectors are given by $\mathbf{x}=(x,y,z)$ and $\mathbf{v}=(u,v,\omega)$ respectively.

Thus, all the information required to describe the system has been compressed in a single scalar function, the probability density function – pdf – $\Psi(\mathbf{x},\mathbf{v},t)$ and the only price to be paid concerns its multi-dimensional character.

Despite the high compactness of such kinetic theory description, it is not useful without an equation governing the evolution of the joint distribution function $\Psi(\mathbf{x},\mathbf{v},t)$ from the prescribed initial and boundary conditions. The equation governing the evolution of the distribution function results from the particle conservation balance in the physical and conformational spaces that reads

$$\frac{\partial \Psi}{\partial t} + \nabla_x \cdot (\mathbf{q}_x) + \nabla_v \cdot (\mathbf{q}_v) = S, \tag{4.1}$$

where $\nabla_x \cdot (\bullet)$ and $\nabla_v \cdot (\bullet)$ denote the divergence linear differential operator in the physical (space) and conformational (velocity) coordinates respectively, and the source S is called collision term. The convective fluxes in both spaces, the physical $\mathbf{q}_x$ and the conformational $\mathbf{q}_v$ ones, are given by

$$\begin{cases} \mathbf{q}_x = \dot{\mathbf{x}}\,\Psi = \mathbf{v}\Psi \\ \\ \mathbf{q}_v = \dot{\mathbf{v}}\,\Psi = \mathbf{a}\Psi \end{cases}, \tag{4.2}$$

with $\mathbf{a}$ the acceleration field. With this notation the balance equation reads:

$$\frac{\partial \Psi}{\partial t} + \nabla_x \cdot (\mathbf{v}\Psi) + \nabla_v \cdot (\mathbf{a}\Psi) = S. \tag{4.3}$$

Obviously, before solving Eq. (4.3) one needs to specify both the collision term and the acceleration field, as well as the initial and boundary conditions. The velocity field $\mathbf{v}$ that appears in the second term does not require any specific treatment because in the present approach the velocity components are in fact coordinates, like space and time. The collision term depends on the considered physics. In turn

the acceleration field can be derived from the fact that the population that we are considering consists of a set of particles with electrical charge that are interacting through the Coulomb's potential. In the kinetic theory description localized charges are substituted by the charge distribution

$$Q(\mathbf{x},t) = Z \int_{\mathbb{R}^3} \Psi(\mathbf{x},\mathbf{v},t) d\mathbf{v}, \tag{4.4}$$

where Z is the total charge in the system, as the following expression proves:

$$\int_{\mathbb{R}^3} Q(\mathbf{x},t) d\mathbf{x} = Z \int_{\mathbb{R}^3} \left(\int_{\mathbb{R}^3} \Psi(\mathbf{x},\mathbf{v},t) d\mathbf{v} \right) d\mathbf{x} = Z, \quad \forall t. \tag{4.5}$$

Now, an electrostatic potential $V(\mathbf{x},t)$ can be associated with this charge distribution $Q(\mathbf{x},t)$, that verifies the elliptic partial differential equation

$$\nabla_x^2 V(\mathbf{x},t) = Q(\mathbf{x},t); \quad \forall t, \tag{4.6}$$

where ∇_x denotes the gradient linear differential operator with respect to the space coordinates $\mathbf{x}$. From the electrostatic potential that results from the solution of Eq. (4.6) we can compute the electrical field $\mathbf{E}(\mathbf{x},t)$

$$\mathbf{E}(\mathbf{x},t) = -\nabla_x V(\mathbf{x},t), \tag{4.7}$$

from which we can easily derive the expression of the force $\mathbf{F}(\mathbf{x},t)$ acting on a volume $d\Omega$ located at point $\mathbf{x}$ (at time t)

$$\mathbf{F}(\mathbf{x},t) = \mathbf{E}(\mathbf{x},t) Q(\mathbf{x},t) d\Omega, \tag{4.8}$$

that gives the acceleration

$$a(\mathbf{x},t) = \frac{\mathbf{F}(\mathbf{x},t)}{\rho(\mathbf{x},t) d\Omega} = -\nabla_x V(\mathbf{x},t) \frac{Q(\mathbf{x},t)}{\rho(\mathbf{x},t)}, \tag{4.9}$$

where $\rho(\mathbf{x},t)$ is the density,

$$\rho(\mathbf{x},t) = M \int_{\mathbb{R}^3} \Psi(\mathbf{x},\mathbf{v},t) d\mathbf{v}, \tag{4.10}$$

with M the total mass in the system.

Thus, the model can be summarized by the following equations

$$\begin{cases} \frac{\partial \Psi}{\partial t} + \nabla_x \cdot (\mathbf{v}\Psi) + \nabla_v \cdot (\mathbf{a}\Psi) = S \\ \mathbf{a}(\mathbf{x},t) = -\nabla_x V(\mathbf{x},t) \frac{Q(\mathbf{x},t)}{\rho(\mathbf{x},t)} \\ Q(\mathbf{x},t) = Z \int_{\mathbb{R}^3} \Psi(\mathbf{x},\mathbf{v},t) d\mathbf{v} \\ \rho(\mathbf{x},t) = M \int_{\mathbb{R}^3} \Psi(\mathbf{x},\mathbf{v},t) d\mathbf{v} \\ \nabla_x^2 V(\mathbf{x},t) = Q(\mathbf{x},t) \end{cases} . \tag{4.11}$$

This model has been widely applied for modeling quantum gases (plasma) and it is known as the Vlasov-Poisson-Boltzmann model.

If the particles are not charged the acceleration vanishes, i.e. $\mathbf{a}(\mathbf{x},t) = \mathbf{0}$ except during the instantaneous collisions, then the steady solution results in the Maxwell-Boltzmann distribution which is considered as the equilibrium distribution Ψ_{eq}.

In fact, the equilibrium distribution allows to define, within the so-called BFK (Bhatnagar-Gross-Krook) model, the collision term as

$$S = -\nu_{ref}(\Psi - \Psi_{eq}), \tag{4.12}$$

where ν_{eq} is the inverse of a characteristic time. Now, in absence of electrical charge, the equation governing the evolution of the distribution could be written in the form:

$$\frac{\partial \Psi}{\partial t} + \nabla_x \cdot (\mathbf{v}\Psi) = -\nu_{eq}(\Psi - \Psi_{eq}). \tag{4.13}$$

From this analysis we can conclude that the use of extremely large populations of particles characteristic of discrete simulation techniques (MD or BD) can be replaced by the solution of a continuous model. However the solution of the resulting partial differential equation is a tricky issue because of its hyperbolic character and its multidimensionality. In [21] authors considered the use of separated representations for alleviating the just referred difficulties.

Lattice-Boltzmann approaches can be viewed as an attempt to circumvent both difficulties and they attracted the interest of many researchers in the last decades. A brief summary is given in Section 4.2.2, and for additional details the interested reader can refer to [48] and the references therein.

4.2.1 Hydrodynamic equations

When considering the Boltzmann equation

$$\frac{\partial \Psi}{\partial t} + \nabla_x \cdot (\mathbf{v}\Psi) = S(\mathbf{x},\mathbf{v},t), \tag{4.14}$$

its solution $\Psi(\mathbf{x},\mathbf{v},t)$ allows to define the macroscopic quantities $\rho(\mathbf{x},t)$ and $\mathbf{u}(\mathbf{x},t)$, the density and the macroscopic velocity respectively, from

$$\rho(\mathbf{x},t) = \int_{\mathbb{R}} \Psi(\mathbf{x},\mathbf{v},t) d\mathbf{v}, \tag{4.15}$$

and

$$\rho(\mathbf{x},t)\mathbf{u}(\mathbf{x},t) = \int_{\mathbb{R}} \mathbf{v}\Psi(\mathbf{x},\mathbf{v},t) d\mathbf{v}. \tag{4.16}$$

The pressure tensor $\mathbf{P}$, that contains the scalar pressure and the viscous stress results from

$$\mathbf{P}(\mathbf{x},t) = \int_{\mathbb{R}} (\mathbf{v}-\mathbf{u}(\mathbf{x},t)) \otimes (\mathbf{v}-\mathbf{u}(\mathbf{x},t))\ \Psi(\mathbf{x},\mathbf{v},t) d\mathbf{v}, \tag{4.17}$$

that leads to

$$\mathbf{P}(\mathbf{x},t) = -\rho(\mathbf{x},t)\ \mathbf{u}(\mathbf{x},t) \otimes \mathbf{u}(\mathbf{x},t) + \int_{\mathbb{R}} \mathbf{v} \otimes \mathbf{v}\ \Psi(\mathbf{x},\mathbf{v},t) d\mathbf{v}. \tag{4.18}$$

The mass and momentum conservation imply

$$\begin{cases} \int_{\mathbb{R}} S(\mathbf{x},\mathbf{v},t) d\mathbf{v} = 0 \\ \int_{\mathbb{R}} \mathbf{v} S(\mathbf{x},\mathbf{v},t) d\mathbf{v} = 0 \end{cases}. \tag{4.19}$$

Now, in order to obtain the first hydrodynamic equation it suffices to integrate the Boltzmann equation as follows

$$\int_{\mathbb{R}} \left(\frac{\partial \Psi}{\partial t} + \nabla_x \cdot (\mathbf{v}\Psi) - S \right) d\mathbf{v} = 0, \tag{4.20}$$

that implies

$$\frac{\partial \rho}{\partial t} + \nabla_x \cdot (\rho \mathbf{u}) = 0, \tag{4.21}$$

that corresponds to the standard continuity equation. Now, by multiplying the Boltzmann equation by $\mathbf{v}$ and then integrating in the velocity space it results

$$\int_{\mathbb{R}} \mathbf{v} \left(\frac{\partial \Psi}{\partial t} + \nabla_x \cdot (\mathbf{v}\Psi) - S \right) d\mathbf{v} = \mathbf{0}, \tag{4.22}$$

that operating and making use of the previous definitions becomes

$$\frac{\partial (\rho \mathbf{u})}{\partial t} + \nabla_x \cdot (\rho \mathbf{u} \otimes \mathbf{u}) + \nabla_x \cdot \mathbf{P} = \mathbf{0}. \tag{4.23}$$

In order to make explicit the macroscopic expression of the pressure tensor $\mathbf{P}$ the simplest route consists in using the Chapman-Enskog expansion that expresses the distribution function $\Psi(\mathbf{x},\mathbf{v},t)$ from the asymptotic expansion

$$\Psi = \sum_{i=0}^{\infty} \varepsilon^i \Psi^{(i)}. \tag{4.24}$$

Then this expansion is injected into the Boltzmann equation using the BFK model of the collision term according to

$$\frac{\partial(\Psi^{(0)} + \varepsilon\Psi^{(1)} + \cdots)}{\partial t} + \mathbf{v}\cdot\nabla_x\left(\Psi^{(0)} + \varepsilon\Psi^{(1)} + \cdots\right) = \frac{\left(\Psi^{(0)} + \varepsilon\Psi^{(1)} + \cdots\right) - \Psi^{eq}}{\tau}, \tag{4.25}$$

with $\varepsilon\Theta\tau$. By identifying the terms at the different orders we obtain:

- Order ε^{-1}:
$$\Psi^{(0)} = \Psi^{eq} \tag{4.26}$$
.
- Order ε^0:
$$\frac{\partial\Psi^{(0)}}{\partial t} + \mathbf{v}\cdot\nabla_x\Psi^{(0)} = \Psi^{(1)}. \tag{4.27}$$
- Order ε^1:
$$\frac{\partial\Psi^{(1)}}{\partial t} + \mathbf{v}\cdot\nabla_x\Psi^{(1)} = \Psi^{(2)}, \tag{4.28}$$
and so on for the next orders.

The first order approximation of the pressure tensor $\mathbf{P}^{(0)}$ is obtained by considering the zero order distribution function $\Psi^{(0)}$ that according to the Chapman-Enskog expansion just discussed corresponds to the equilibrium Maxwell-Boltzmann distribution $\Psi^{eq}(\mathbf{v})$ and consequently

$$\mathbf{P}^{(0)}(\mathbf{x},t) = \int_{\mathbb{R}} (\mathbf{v}-\mathbf{u}(\mathbf{x},t)) \otimes (\mathbf{v}-\mathbf{u}(\mathbf{x},t))\ \Psi^{eq}(\mathbf{v}) d\mathbf{v} = K_b T \rho(\mathbf{x},t), \tag{4.29}$$

that injected into Eq. (4.23) leads to the Euler equation.

The second order approximation proceeds from

$$\mathbf{P}^{(1)}(\mathbf{x},t) = \int_{\mathbb{R}} (\mathbf{v}-\mathbf{u}(\mathbf{x},t)) \otimes (\mathbf{v}-\mathbf{u}(\mathbf{x},t))\ \Psi^{(1)}(\mathbf{x},\mathbf{v},t) d\mathbf{v}, \tag{4.30}$$

that according to the Chapman-Enskog expansion just discussed results

$$\Psi^{(1)} = \frac{\partial\Psi^{(0)}}{\partial t} + \mathbf{v}\cdot\nabla_x\Psi^{(0)}, \tag{4.31}$$

with $\Psi^{(0)} = \Psi^{eq}$. It finally results

$$\mathbf{P}^{(1)}(\mathbf{x},t) = 2K_b T\rho\tau(\nabla_x\mathbf{u} + (\nabla_x\mathbf{u})^T). \tag{4.32}$$

Defining the viscosity $\mu = K_b T \rho \tau$, and considering $\mathbf{P} = \mathbf{P}^{(0)} + \mathbf{P}^{(1)}$ into Eq. (4.23) the Navier-Stokes equation is obtained.

4.2.2 The Lattice Boltzmann Method – LBM

The use of the LBM provides many of the advantages of molecular dynamics, including clear physical pictures, easy implementation, and fully parallel algorithms. The basic premise for using this simplified kinetic-type method for macroscopic fluid flows is that the macroscopic dynamics of a fluid is the result of the collective behavior of many microscopic particles in the system and that the macroscopic dynamics is not sensitive to the underlying details in microscopic physics. The LBM ancestor is the lattice gas automata which is constructed as a simplified, fictitious molecular dynamic in which space, time, and particle velocities are all discrete. It consists of a regular lattice with particles residing on the nodes. Starting from an initial state, the configuration of particles at each time step evolves in two sequential sub-steps: (i) streaming, in which each particle moves to the nearest node in the direction of its velocity, and (ii) collision, which occurs when particles arriving at a node interact and change their velocity directions according to specified rules. The lattice Boltzmann method considers a number of velocity directions depending on the considered cell and a velocity value associated to each one of these directions allowing to reach the neighbor location in the considered time step.

We consider the Botzmann equation within the BFK (Bhatnagar-Gross-Krook) modeling of the collision term,

$$\frac{\partial \Psi}{\partial t} + \nabla_x \cdot (\mathbf{v}\Psi) = -\nu_{eq}(\Psi - \Psi_{eq}), \tag{4.33}$$

and consider a regular grid, the so-called lattice, of size Δx. For the sake of simplicity we consider the two-dimensional model where the particles are constrained to occupy the nodes of the lattice. This fact constitutes the first simplification. The second assumption restricts a particle to stream in a finite number of possible directions, 9 when considering the lattice node illustrated in Fig. 4.1, usually referred as D2Q9. These velocities are denoted by vectors $\mathbf{e}_i$, $i = 1, \cdots, 8$. The reduction accomplished is quite impressive: an infinity of points $\mathbf{x}$, each of them having an infinity of directions and magnitude of the possible velocities, has been reduced to the nodes in the lattice, with only 8 possible directions and only one velocity magnitude associated to each direction, 1 for directions 1 to 4 and $\sqrt{2}$ for directions 5 to 8.

Now, we denote by $\Psi_i(\mathbf{x},t)$ the probability of streaming in direction $\mathbf{e}_i$ with its associated velocity at the lattice point $\mathbf{x}$ and time t. The two steps in the Lattice-Boltzmann simulations are the streaming and the collision that combined read, $\forall i$

$$\Psi_i(\mathbf{x} + c\Delta t \mathbf{e}_i, t + \Delta t) - \Psi_i(\mathbf{x},t) = -\nu_{eq}\left(\Psi_i(\mathbf{x},t) - \Psi_i^{eq}(\mathbf{x},t)\right), \tag{4.34}$$

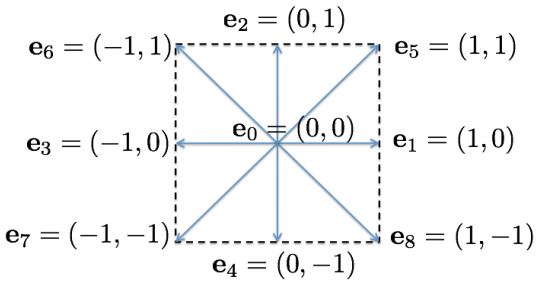

Fig. 4.1 D2Q9 lattice node

where the left-hand side represents the streaming while the right-hand side the collision, and c is the so-called lattice speed, $c = \frac{\Delta x}{\Delta t}$.

The macroscopic density ρ and velocity $\mathbf{u}$ read

$$\rho(\mathbf{x},t) = \sum_{i=0}^{8} \Psi_i(\mathbf{x},t), \tag{4.35}$$

and

$$\mathbf{u}(\mathbf{x},t) = \frac{1}{\rho(\mathbf{x},t)} \sum_{i=0}^{8} c\Psi_i(\mathbf{x},t)\mathbf{e}_i, \tag{4.36}$$

respectively.

Now, when considering single phase flows, the D2Q9 lattice and the BGK collision term, the equilibrium distribution Ψ_i^{eq} reads

$$\Psi_i^{eq} = \rho\omega_i + \rho s_i(\mathbf{u}(\mathbf{x},t)), \tag{4.37}$$

where

$$s_i(\mathbf{u}) = \omega_i \left(3\frac{\mathbf{e}_i \cdot \mathbf{u}}{c} + \frac{9}{2}\frac{(\mathbf{e}_i \cdot \mathbf{u})^2}{c^2} - \frac{3}{2}\frac{\mathbf{u}\cdot\mathbf{u}}{c^2} \right), \tag{4.38}$$

with the weights given by

$$\omega_i = \begin{cases} \frac{4}{9} & i = 0 \\ \frac{1}{9} & i = 1,\cdots,4 \\ \frac{1}{36} & i = 5,\cdots,8 \end{cases}. \tag{4.39}$$

To obtain these expressions it suffices to define an equilibrium distribution which fulfills the macroscopic definitions $\sum_i \Psi_i^{eq} = \rho$, $\sum_i \Psi_i^{eq}(c\mathbf{e}_i - \mathbf{u}) = \mathbf{0}$, etc, and from them, to identify the different terms Ψ_i^{eq}.

The simulation algorithm can be summarized as follows:

1. Initialize Ψ_i, and from it compute ρ, $\mathbf{u}$ and then Ψ_i^{eq};
2. *Streaming step:* From Ψ_i compute $\Psi_i^*(\mathbf{x} + c\Delta t\mathbf{e}_i, t + \Delta t) = \Psi(\mathbf{x},t)$;
3. From Ψ_i^* compute ρ and $\mathbf{u}$, and from both Ψ_i^{eq};

4. *Collision step:* Update the distribution Ψ_i from $\Psi_i = \Psi_i^* - \nu(\Psi_i^* - \Psi_i^{eq})$.

The main issues related to the use of this procedure (very simple at first glance) are the enforcement of Dirichlet boundary conditions and the calculation of the expression of the equilibrium distribution for complex or multi-phase flows. The interested reader can refer to the vast existing bibliography on these topics.

4.3 Kinetic theory description of some complex fluids

Over the last decades, an increasing number of functional and structural parts, made so far with metals, has been progressively reengineered by replacing metallic materials by polymers, reinforced polymers and composites. The motivation for this substitution may be the weight reduction, the simpler, cheaper or faster forming process, or the ability to exploit additional functionalities. The fillers usually employed cover a broad range involving many scales: (i) the nanometer scale (e.g. carbon nanotubes, graphene, fullerene, nanodiamonds); (ii) the micrometer to the millimeter scale (particles and short fibers); (iii) the centimeter scale of fibers used in SMC and BMC composite processes; and finally (iv) the macroscopic scale where fibrous reinforcements are made of continuous fibers arranged in bundles. When load-bearing capacities are especially looked for, continuous fiber reinforced polymers are selected. In that case, the impregnation of the reinforcement with a low viscosity polymer involves the flow of a Newtonian or non-Newtonian fluid in the complex multi-scale microstructure related to the fiber and tow arrangement. Reinforced polymers are selected instead of high performance polymers of equivalent properties since the latter are generally more expensive. When looking for functional properties, the use of nano-charges opens a wide spectrum of possibilities but also raises new challenges, such as dispersion of charges into the polymer matrix and occurrence of aggregation and disaggregation mechanisms. Suspensions of practical interest involve many scales and many concentration regimes, the latter ranging from dilute to highly concentrated.

In what follows we are addressing many of the just referred scenarios. We start addressing the modeling of suspensions involving rigid rods where the Brownian effects are neglected. For this purpose we consider a suspending medium consisting of a Newtonian fluid of viscosity η in which there are suspended rigid and non-Brownian rods. We assume as first approximation that their presence and orientation do not affect the flow kinematics that is defined by the velocity field $\mathbf{v}(\mathbf{x},t)$, that allows defining the velocity gradient, rate of strain and vorticity tensors, $\nabla\mathbf{v}$, $\mathbf{D}$ and Ω respectively, with $\mathbf{D}$ and Ω the symmetric and skew-symmetric components of the velocity gradient respectively, i.e.

$$\mathbf{D} = \frac{1}{2}\left(\nabla\mathbf{v} + (\nabla\mathbf{v})^T\right), \tag{4.40}$$

and

$$\Omega = \frac{1}{2}\left(\nabla \mathbf{v} - (\nabla \mathbf{v})^T\right). \tag{4.41}$$

In what follows we consider the following tensor products:

- if $\mathbf{a}$ and $\mathbf{b}$ are first order tensors then the single contraction "$\cdot$" reads $(\mathbf{a}\cdot\mathbf{b}) = a_j\, b_j$ (Einstein summation convention);
- if $\mathbf{a}$ and $\mathbf{b}$ are first order tensors then the dyadic product "$\otimes$" reads $(\mathbf{a}\otimes\mathbf{b})_{jk} = a_j\, b_k$;
- if $\mathbf{a}$ and $\mathbf{b}$ are first order tensors then the cross product "$\times$" reads $(\mathbf{a}\times\mathbf{b})_j = \varepsilon_{jmn}\, a_m\, b_n$ (Einstein summation convention) with ε_{jmn} the components of the Levi-Civita tensor ε (also known as permutation tensor);
- if $\mathbf{a}$ and $\mathbf{b}$ are respectively second and first order tensors then the single contraction "$\cdot$" reads $(\mathbf{a}\cdot\mathbf{b})_j = a_{jm}\, b_m$ (Einstein summation convention);
- if $\mathbf{a}$ and $\mathbf{b}$ are second order tensors then the single contraction "$\cdot$" reads $(\mathbf{a}\cdot\mathbf{b})_{jk} = a_{jm}\, b_{mk}$ (Einstein summation convention);
- if $\mathbf{a}$ and $\mathbf{b}$ are second order tensors then the double contraction ':" reads $(\mathbf{a}:\mathbf{b}) = a_{jk}\, b_{kj}$ (Einstein summation convention);

4.3.1 Dilute suspensions of non-Brownian rods

To address the modeling of suspensions involving rigid rods while neglecting the Brownian effects, we consider nine different bricks that constitutes the multiscale description of such suspensions: three at the microscopic scale, three at the mesoscopic level and three at the macroscopic scale, all them revisited in what follows.

Microscopic scale: Particle conformation

The conformation of each rod of length $2L$ can be described from its orientation, the last expressed from the unit vector $\mathbf{p}$ located at the rod center of gravity $\mathbf{G}$ and aligned along the rod axis. Despite the fact of using the concept of rod center of gravity, the rod mass can be neglected and with it all the inertia effects.

Microscopic scale: Particle conformation evolution

The equation governing the time evolution of the particle conformation $\dot{\mathbf{p}}$ can be derived by considering the system illustrated in Fig. 4.5 consisting of a rod and two beads located at both rod ends where we assume that hydrodynamic forces act. We assume that the forces $\mathbf{F}$ that act on each bead scale with the difference of velocities between the fluid and the bead, the first one given by $\mathbf{v}_0 + \nabla\mathbf{v}\cdot\mathbf{p}L$ and the second one by $\mathbf{v}_G + \dot{\mathbf{p}}L$. Thus, force $\mathbf{F}(\mathbf{p}L)$ reads:

$$\mathbf{F}(\mathbf{p}L) = \xi(\mathbf{v}_0 + \nabla\mathbf{v}\cdot\mathbf{p}L - \mathbf{v}_G - \dot{\mathbf{p}}L), \tag{4.42}$$

where ξ is the friction coefficient, $\mathbf{v}_0$ the fluid velocity at the rod's center of gravity (assumed unperturbed by the rod presence and orientation) and $\mathbf{v}_G$ the velocity of the center of gravity.

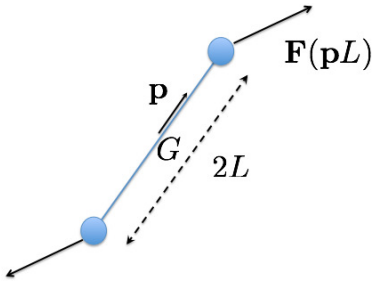

Fig. 4.2 Hydrodynamic forces applying on a rod immersed in a Newtonian fluid

Obviously if $\mathbf{F}(\mathbf{p}L)$ acts on the bead $\mathbf{p}L$, then in the opposite bead $-\mathbf{p}L$ the resulting force reads

$$\mathbf{F}(-\mathbf{p}L) = \xi(\mathbf{v}_0 - \nabla\mathbf{v}\cdot\mathbf{p}L - \mathbf{v}_G + \dot{\mathbf{p}}L). \tag{4.43}$$

Adding Eqs. (4.42) and (4.43) and enforcing the forces balance neglecting inertia effects (the rods mass is assumed negligible) it results

$$\mathbf{F}(\mathbf{p}L) + \mathbf{F}(-\mathbf{p}L) = 2\xi(\mathbf{v}_0 - \mathbf{v}_G) = \mathbf{0}, \tag{4.44}$$

than implies $\mathbf{v}_0 = \mathbf{v}_G$, that is, the rod center of gravity is moving with the fluid velocity. To simplify the notation from now on we consider $\mathbf{F} = \mathbf{F}(\mathbf{p}L)$ and $\mathbf{F}(-\mathbf{p}L) = -\mathbf{F}$.

As the resulting torque must also vanish, the only possibility is that force $\mathbf{F}$ acts along $\mathbf{p}$, that is $\mathbf{F} = \lambda\mathbf{p}$, with $\lambda \in \mathbb{R}$. Thus we can write

$$\lambda\mathbf{p} = \xi L(\nabla\mathbf{v}\cdot\mathbf{p} - \dot{\mathbf{p}}). \tag{4.45}$$

Premultiplying Eq. (4.45) by $\mathbf{p}$ and taking into account that $\mathbf{p}\cdot\mathbf{p} = 1$ and consequently $\mathbf{p}\cdot\dot{\mathbf{p}} = 0$, it results

$$\lambda = \xi L(\nabla\mathbf{v} : (\mathbf{p}\otimes\mathbf{p})), \tag{4.46}$$

where $\nabla\mathbf{v} : (\mathbf{p}\otimes\mathbf{p}) \equiv \mathbf{p}^T\cdot\nabla\mathbf{v}\cdot\mathbf{p}$ (both expressions $\nabla\mathbf{v} : (\mathbf{p}\otimes\mathbf{p})$ and $\mathbf{p}^T\cdot\nabla\mathbf{v}\cdot\mathbf{p}$ will be used in what follows indifferently).

Coming back to Eq. (4.45) and using Eq. (4.46) we obtain

$$\xi L(\nabla\mathbf{v} : (\mathbf{p}\otimes\mathbf{p}))\,\mathbf{p} = \xi L(\nabla\mathbf{v}\cdot\mathbf{p} - \dot{\mathbf{p}}), \tag{4.47}$$

from which it results finally that the rotary velocity corresponds to the Jeffery equation for infinite aspect ratio ellipsoids (rods) [34]

(4.48)

$$\dot{\mathbf{p}} = \nabla\mathbf{v}\cdot\mathbf{p} - (\nabla\mathbf{v} : (\mathbf{p}\otimes\mathbf{p}))\,\mathbf{p},$$

or its equivalent form

$$\dot{\mathbf{p}} = \nabla\mathbf{v}\cdot\mathbf{p} - \left(\mathbf{p}^T\cdot\nabla\mathbf{v}\cdot\mathbf{p}\right)\mathbf{p}, \tag{4.49}$$

where it can be noticed that the rod kinematics does not contain size effects.

Microscopic scale: Particle contribution to the stress

The forces acting at the rods ends $\mathbf{p}L$ and $-\mathbf{p}L$ result respectively $\lambda\mathbf{p}$ and $-\lambda\mathbf{p}$, both directed along the rod direction and by construction auto-equilibrated.

With λ given by Eq. (4.46) it results

$$\mathbf{F}(\mathbf{p}L) = \xi L(\nabla\mathbf{v} : (\mathbf{p}\otimes\mathbf{p}))\,\mathbf{p}, \tag{4.50}$$

whose contribution to the stress τ^p, by applying the Kramer's formula (also known as virial stress), results

$$\tau^p = \xi L^2(\nabla\mathbf{v} : (\mathbf{p}\otimes\mathbf{p}))\,\mathbf{p}\otimes\mathbf{p}, \tag{4.51}$$

that can be rewritten as

$$\tau^p = \xi L^2\,\nabla\mathbf{v} : (\mathbf{p}\otimes\mathbf{p}\otimes\mathbf{p}\otimes\mathbf{p}). \tag{4.52}$$

From Eq. (4.52) one could infer that rheology contains size effects because the presence of factor L^2 in the particle contribution to the stress. To prove that size effects also disappears when addressing rheology we consider the traction applied on the rod-end $\mathbf{T}$ that by considering a Newtonian behavior writes $\mathbf{T} = 2\eta\mathbf{D}\cdot\mathbf{p}$. By writing the objective stress related to the rod rotation $2\eta(\dot{\mathbf{p}} - \Omega\cdot\mathbf{p})$ and enforcing that the resulting force aligns along the direction $\mathbf{p}$, we obtain again the Jeffery's equation. In order to obtain the same expression for the stress it suffices considering $\xi \propto \frac{\eta}{L^2}$. Thus we can conclude that size effects are absent in Eq. (4.52).

Mesoscopic scale: Population description

There are two natural descriptions of a population of rods at a mesoscopic level:

- The first consists in specifying each rod orientation by considering the unit vector aligned along its axis, that is, by considering $\mathbf{p}_i$, $i = 1,\cdots,N$. As discussed later the main drawback related to such approach lies in the necessity of tracking the evolution of each "computational" rod by solving the corresponding Jeffery equation (4.49), and even if conceptually there is no major difficulty, the computing cost could be excessive in most practical applications.

- The second approach for describing such a population lies in the introduction of the probability distribution function – pdf – $\Psi(\mathbf{x},t,\mathbf{p})$ given the fraction of rods that a position $\mathbf{x}$ and time t are oriented along direction $\mathbf{p}$.

Despite the fact that both mesoscopic models involve the same physics and richness of description, the main advantage of the second one is the manipulation of a scalar continuous function instead of the discrete description involved in the first approach. The price to be paid when using the description based on the use of the pdf is its inherent multidimensionality, because in that framework the pdf depends on the standard space and time coordinates, $\mathbf{x}$ and t respectively, and also on the conformation coordinates that the microstructural description involves, in the present case $\mathbf{p}$.

Mesoscopic scale: Description of the population evolution

- When the population is described from the individuals composing it, whose conformation is given by vectors $\mathbf{p}_i$, $i = 1,\cdots,N$, the evolution of each one is given by the Jeffery equation (4.49), that reads

$$\dot{\mathbf{p}}_i = \nabla\mathbf{v}\cdot\mathbf{p}_i + (\nabla\mathbf{v} : (\mathbf{p}_i\otimes\mathbf{p}_i))\,\mathbf{p}_i, \quad \forall i = 1,\cdots,N. \tag{4.53}$$

- The alternative description consists of using the pdf $\Psi(\mathbf{x},t,\mathbf{p})$ that verifies the normality condition

$$\int_{\mathscr{S}} \Psi(\mathbf{x},t,\mathbf{p})\, d\mathbf{p} = 1; \quad \forall\mathbf{x},\ \forall t. \tag{4.54}$$

In order to use it, one needs to derive the equation governing the evolution of the orientation distribution function Ψ, that is related to the rods conservation balance, that reads

$$\frac{\partial\Psi}{\partial t} + \nabla_x\cdot(\dot{\mathbf{x}}\,\Psi) + \nabla_p\cdot(\dot{\mathbf{p}}\,\Psi) = 0, \tag{4.55}$$

where for inertialess rods, with length L smaller that the characteristic flow length, $\dot{\mathbf{x}} = \mathbf{v}(\mathbf{x},t)$ and the rods rotary velocity is given by Jeffery's equation (4.49). The resulting balance is known as the orientation Fokker-Planck equation.
The price to pay is the increase of the model dimensionality, because the orientation distribution is defined in a high-dimensional domain consisting of 6 dimensions in the general 3D case, i.e. $\Psi : (\mathbf{x},t,\mathbf{p}) \to \mathbb{R}^+$.

Mesoscopic scale: Contribution of the particles population to the stress

Again we consider the two alternative descriptions:

- When the population is described in a discrete manner, by specifying the different rods orientations $\mathbf{p}_i$, the contributions of rods to the suspension stress is calculated by adding their individual effects, given by Eq. (4.52), that is

$$\tau = \sum_{i=1}^{N} \tau^i = \sum_{i=1}^{N} \xi L^2 \, \nabla \mathbf{v} : (\mathbf{p}_i \otimes \mathbf{p}_i \otimes \mathbf{p}_i \otimes \mathbf{p}_i). \tag{4.56}$$

- When the population is described from the pdf $\Psi(\mathbf{x}, t, \mathbf{p})$ the sum in Eq. (4.56) is replaced by an integral in the conformation space $\mathscr{S}$:

$$\tau = \int_{\mathscr{S}} \tau^p \, \Psi(\mathbf{p}) \, d\mathbf{p} = 2\eta N_p \int_{\mathscr{S}} \nabla \mathbf{v} : (\mathbf{p} \otimes \mathbf{p} \otimes \mathbf{p} \otimes \mathbf{p}) \, \Psi(\mathbf{p}) \, d\mathbf{p} =$$

$$2\eta N_p \nabla \mathbf{v} : \int_{\mathscr{S}} \mathbf{p} \otimes \mathbf{p} \otimes \mathbf{p} \otimes \mathbf{p} \, \Psi(\mathbf{p}) \, d\mathbf{p}, \tag{4.57}$$

  where the so-called particle number N_p accounts for the particles concentration and where we considered the viscosity instead of the friction coefficient to be consistent with the usual notation.
  By considering the expression of the fourth order orientation tensor

$$\mathbf{A} = \int_{\mathscr{S}} \mathbf{p} \otimes \mathbf{p} \otimes \mathbf{p} \otimes \mathbf{p} \, \Psi(\mathbf{p}) \, d\mathbf{p}, \tag{4.58}$$

  Eq. (4.57) can be rewritten as

$$\tau = 2\eta N_p (\mathbf{A} : \nabla \mathbf{v}), \tag{4.59}$$

  and because the symmetry of tensor $\mathbf{A}$, the extra-stress τ can be expressed from

$$\tau = 2\eta N_p (\mathbf{A} : \mathbf{D}). \tag{4.60}$$

Macroscopic scale: Conformation

As just discussed discrete descriptions are computationally expensive because of the large number of rods that must be considered in order to derive accurate enough model outputs. On the other hand Fokker-Planck based descriptions are rarely considered precisely because the curse of dimensionality that the introduction of conformation coordinates (the rod orientation in the case here considered) implies. Thus standard mesh-based discretization techniques, as finite differences, finite elements or finite volumes, fail when addressing models defined in high-dimensional spaces.

For these reasons, mesoscopic models were coarsened to derive macroscopic models defined in standard physical domains, involving space and time. At the macroscopic scale the orientation distribution function is substituted by its moments for describing the microstructure. Usually macroscopic descriptions of rods suspensions are based on the use of the first two non-vanishing moments, the second, $\mathbf{a}$, and the fourth, $\mathbf{A}$, order moments (the odd moments vanish because the symmetry

of the pdf), the former is given by

$$\mathbf{a} = \int_{\mathscr{S}} \mathbf{p} \otimes \mathbf{p}\ \Psi(\mathbf{p})\ d\mathbf{p}, \tag{4.61}$$

and the latter by Eq. (4.58).

Macroscopic scale: Microstructural evolution

The microstructural evolution described at the macroscopic scale considers the time evolution of the pdf moments. The time evolution of the second order orientation tensor, when replacing $\dot{\Psi}$ by its expression given by the Fokker-Planck equation (4.69), and after integrating by parts, results

$$\dot{\mathbf{a}} = \int_{\mathscr{S}} (\dot{\mathbf{p}} \otimes \mathbf{p} + \mathbf{p} \otimes \dot{\mathbf{p}})\ \Psi\ d\mathbf{p} =$$

$$\int_{\mathscr{S}} (\nabla \mathbf{v} \cdot \mathbf{p} - (\nabla \mathbf{v} : (\mathbf{p} \otimes \mathbf{p}))\ \mathbf{p}) \otimes \mathbf{p}\ \Psi\ d\mathbf{p} +$$

$$\int_{\mathscr{S}} \mathbf{p} \otimes (\nabla \mathbf{v} \cdot \mathbf{p} - (\nabla \mathbf{v} : (\mathbf{p} \otimes \mathbf{p}))\ \mathbf{p})\ \Psi\ d\mathbf{p} =$$

$$\nabla \mathbf{v} \cdot \mathbf{a} + \mathbf{a} \cdot (\nabla \mathbf{v})^T - 2\ \mathbf{A} : \nabla \mathbf{v}, \tag{4.62}$$

that depends on the fourth order moment $\mathbf{A}$. The time derivative of the fourth order moment, using the same rationale, implies the sixth order one $\mathscr{A}$, and so on.

Another possibility for deducing Eq. (4.62) lies in applying the rationale followed for deriving the hydrodynamic equations in Section 4.2.1. Thus, we multiply the Fokker-Planck equation (4.69) by $\mathbf{p} \otimes \mathbf{p}$ and integrate on the unit ball surface $\mathscr{S}$, making use of the integration by parts for the term involving $\nabla_p(\dot{p}\Psi)$. This procedure will be considered later when addressing polymeric systems.

Thus, if we consider the microstructure described from '$\mathbf{a}$" a closure relation is needed in order to express the fourth order moment "$\mathbf{A}$" as a function of the lower order moments ($\mathbf{a}$ in the present case). Different closure relations have been introduced and widely used [12]. When considering for example the quadratic closure relation (that is only exact when all the rods are locally aligned in the same direction) the fourth order moment results

$$\mathbf{A} \approx \mathbf{a} \otimes \mathbf{a}, \tag{4.63}$$

that allows writing

$$\dot{\mathbf{a}} \approx \nabla \mathbf{v} \cdot \mathbf{a} + \mathbf{a} \cdot (\nabla \mathbf{v})^T - 2\ (\nabla \mathbf{v} : \mathbf{a})\ \mathbf{a}, \tag{4.64}$$

or invoking again symmetry considerations

$$\dot{\mathbf{a}} \approx \nabla \mathbf{v} \cdot \mathbf{a} + \mathbf{a} \cdot (\nabla \mathbf{v})^T - 2\ (\mathbf{D} : \mathbf{a})\ \mathbf{a}. \tag{4.65}$$

Macroscopic scale: Moment based stress

We obtained previously the expression of the rods population contribution to the stress

$$\tau = 2\eta N_p(\mathbf{A} : \nabla \mathbf{v}), \tag{4.66}$$

that implies the use of the fourth order moment $\mathbf{A}$. When $\mathbf{A}$ is calculated from the pdf Ψ by using (4.58) within the mesoscopic framework there is no closure issues. However, when one proceed at the macroscopic scale in which the pdf is not available anymore, a closure relation must be considered for either

- writing $\mathbf{A}$ from the knowledge of $\mathbf{a}$, the last calculated by integrating (4.62) with an appropriate closure relation (e.g. Eq. (4.64) when considering the quadratic closure),

or

- calculating $\mathbf{A}$ by solving the equation that governs its time evolution in which as just commented the sixth order moment appears requiring again an appropriate closure.

The first route is the simplest one and the most used in practice, that leads

$$\tau = 2\eta N_p(\mathbf{A}^{cr}(\mathbf{a}) : \nabla \mathbf{v}), \tag{4.67}$$

where the superscript 'cr" refers to the use of an appropriate closure relationship.

When considering the quadric closure the stress writes:

$$\tau = 2\eta N_p(\mathbf{a} : \nabla \mathbf{v})\mathbf{a} = 2\eta N_p(\mathbf{a} : \mathbf{D})\mathbf{a}. \tag{4.68}$$

4.3.2 On the solution of the Fokker-Planck equation

As discussed in the previous section the solution of the Fokker-Planck equation seems a real issue when using well experienced mesh-based discretization techniques due to the curse of dimensionality that it implies. As this issue is a recurrent difficulty in all the models treated in this chapter, before moving on in the description of other kinetic theory models, we are briefly discussing different simulation alternatives.

Since kinetic theory descriptions involve a probability distribution function depending on space, time and a number of conformational coordinates, the associated Fokker-Planck equations suffer the so-called curse of dimensionality typical of problems defined in highly dimensional spaces.

Thus, mesh-based discretization techniques fail for discretizing the problem because the number of degrees of freedom involved in a mesh or grid increases exponentially with the space dimension.

In what follows, we consider some alternatives to standard mesh-based discretization that are able to address the solution of Fokker-Planck equations associated with kinetic theory descriptions.

We consider, without loss of generality, a generic Fokker-Planck equation involving the pdf $\Psi(\mathbf{x},t,\mathbf{a})$ where here $\mathbf{a}$ represents a set of arbitrary conformational coordinates (it is of fundamental importance not to confuse conformational coordinates $\mathbf{a}$ and the orientation tensor considered in the previous section) and diffusion terms are represented by fluxes $\mathbf{q}_x$ and $\mathbf{q}_a$ operating respectively in the physical and conformational spaces:

$$\frac{\partial \Psi}{\partial t} + \nabla_x \cdot (\mathbf{v}\,\Psi) + \nabla_a \cdot (\dot{\mathbf{a}}\,\Psi) = -\nabla_x \cdot \mathbf{q}_x - \nabla_a \cdot \mathbf{q}_a. \tag{4.69}$$

4.3.2.1 Method of particles for solving advection-dominated problems

This technique described in detail in [15] [16] consists in approximating the initial distribution $\Psi(\mathbf{x},t=0,\mathbf{a})$ from $\mathscr{M}$ Dirac's masses $\mathbf{a}_i^0$ at each one of the $\mathscr{Q}$ positions $\mathbf{x}_j^0$:

$$\Psi(\mathbf{x},t=0,\mathbf{a}) = \sum_{j=1}^{\mathscr{Q}} \sum_{i=1}^{\mathscr{M}} \alpha_i^j \; \delta(\mathbf{a}-\mathbf{a}_i^0) \; \delta(\mathbf{x}-\mathbf{x}_j^0). \tag{4.70}$$

This represents a sort of approximation based on $\mathscr{Q}\cdot\mathscr{M}$ computational particles $\mathscr{P}_{ij}$ with initial positions and conformations given by

$$\begin{cases} \mathbf{x}_{ij}^0 = \mathbf{x}_j^0, & i=1,\cdots,\mathscr{M}; \;\; j=1,\cdots,\mathscr{Q} \\ \mathbf{a}_{ij}^0 = \mathbf{a}_i^0, & i=1,\cdots,\mathscr{M}; \;\; j=1,\cdots,\mathscr{Q} \end{cases}, \tag{4.71}$$

and whose position and conformation will be evaluated all along the flow simulation, from which the distribution will be reconstructed.

When considering the purely advective balance equation

$$\frac{\partial \Psi}{\partial t} + \nabla_x \cdot (\mathbf{v}\,\Psi) + \nabla_a \cdot (\dot{\mathbf{a}}\,\Psi) = 0, \tag{4.72}$$

the time evolution of position and conformation of each particle $\mathscr{P}_{ij}$ is calculated by integrating

$$\begin{cases} \mathbf{x}_{ij}(t) = \mathbf{x}_{ij}^0 + \int_{\tau=0}^{\tau=t} \mathbf{v}(\mathbf{x}_{ij}(\tau))\; d\tau \\ \mathbf{a}_{ij}(t) = \mathbf{a}_{ij}^0 + \int_{\tau=0}^{\tau=t} \dot{\mathbf{a}}_{ij}(\mathbf{a}_{ij}(\tau),\mathbf{x}_{ij}(\tau))\; d\tau \end{cases}. \tag{4.73}$$

As the position update only depends on the velocity field, that itself only depends on the position, it can be stressed that particles $\mathscr{P}_{ij}$, $i=1,\cdots,\mathscr{M}$ are following the same trajectory in the physical space, having $\mathbf{x}_j^0$ as departure point.

Now, the orientation distribution at time t can be reconstructed from

$$\Psi(\mathbf{x},t,\mathbf{a}) = \sum_{j=1}^{\mathscr{Q}} \sum_{i=1}^{\mathscr{M}} \alpha_i^j \; \delta(\mathbf{a}-\mathbf{a}_{ij}(t)) \; \delta(\mathbf{x}-\mathbf{x}_{ij}(t)). \tag{4.74}$$

Obviously, smoother representations can be obtained by considering appropriate regularizations of the Dirac's distribution, as the one usually performed within the SPH (Smooth Particles Hydrodynamics) framework [15] [3].

When considering diffusion terms, there are two main routes based on the use of particles, one of stochastic nature, the other fully deterministic.

To illustrate the procedure when models involve diffusion terms, we consider the Fokker-Planck equation

$$\frac{\partial \Psi}{\partial t} + \nabla_x \cdot (\mathbf{v}\,\Psi) + \nabla_a \cdot (\dot{\mathbf{a}}\,\Psi) = -\nabla_x \cdot \mathbf{q}_x - \nabla_a \cdot \mathbf{q}_a, \tag{4.75}$$

where $\mathbf{q}_x$ and $\mathbf{q}_a$ are two diffusive fluxes operating in the physical and conformational spaces respectively, both modeled from a Fick-type law:

$$\begin{cases} \mathbf{q}_x = -\mathbf{D}_x \cdot \nabla_x \Psi \\ \mathbf{q}_a = -\mathbf{D}_a \cdot \nabla_a \Psi \end{cases}. \tag{4.76}$$

- Within the stochastic framework, diffusion terms can be modeled from appropriate random variables within a Lagrangian or a Eulerian description, the last one known as Brownian Configurations Fields (BCF). Both approaches were considered in our former works on the solution of Fokker-Planck equations [16] [17]. Within the Lagrangian stochastic framework and starting from the initial cloud of computational particles $\mathscr{P}_{ij}$ representing the initial distribution $\Psi(\mathbf{x},t=0,\mathbf{a})$, the simplest particles updating reads

$$\begin{cases} \mathbf{x}_{ij}(t_{n+1}) = \mathbf{x}_{ij}(t_n) + \mathbf{v}(\mathbf{x}_{ij}(t_n))\;\Delta t + \mathscr{R}_x(\Delta t) \\ \mathbf{a}_{ij}(t_{n+1}) = \mathbf{a}_{ij}(t_n) + \dot{\mathbf{a}}_{ij}(\mathbf{a}_{ij}(t_n),\mathbf{x}_{ij}(t_n))\;\Delta t + \mathscr{R}_a(\Delta t) \end{cases}, \tag{4.77}$$

  where Δt is the time step and both random updates $\mathscr{R}_x$ and $\mathscr{R}_a$ depend on the chosen time step (see [43] for more details as well as for advanced stochastic integrations).

  Obviously, because of the random effects operating in the physical space, the $\mathscr{M}$ particles initially located at each position $\mathbf{x}_j^0$, $j=1,\cdots,\mathscr{Q}$, will follow different trajectories in the physical space along the simulation. In order to obtain accurate enough results, we must consider a rich enough representation, that is, a large population of particles. For this purpose, we must consider large enough $\mathscr{M}$ and $\mathscr{Q}$. The large number of particles to be tracked seems a disadvantage of the approach at first sight, but it must be noticed that the integration of each particle is completely independent of all the others, making possible the use of HPC on massively parallel computing platforms.
- The technique introduced to treat purely advective equations can be extended to consider diffusion contributions as was described in [3] and that we revisit in what follows, within a fully deterministic approach. Eq. (4.75) can be rewritten as:

$$\frac{\partial \Psi}{\partial t} + \nabla_x \cdot \left(\left(\mathbf{v} + \frac{\mathbf{q}_x}{\Psi} \right) \Psi \right) + \nabla_a \cdot \left(\left((\dot{\mathbf{a}} + \frac{\mathbf{q}_a}{\Psi} \right) \Psi \right) = 0, \tag{4.78}$$

or

$$\frac{\partial \Psi}{\partial t} + \nabla_x \cdot (\tilde{\mathbf{v}} \, \Psi) + \nabla_a \cdot \left(\dot{\tilde{\mathbf{a}}} \, \Psi \right) = 0, \tag{4.79}$$

where the effective velocities $\tilde{\mathbf{v}}$ and $\dot{\tilde{\mathbf{a}}}$ are given by:

$$\begin{cases} \tilde{\mathbf{v}} = \mathbf{v} - \frac{1}{\Psi} \, \mathbf{D}_x \cdot \nabla_x \Psi \\ \dot{\tilde{\mathbf{a}}} = \dot{\mathbf{a}} - \frac{1}{\Psi} \, \mathbf{D}_a \cdot \nabla_a \Psi \end{cases}. \tag{4.80}$$

Now, the integration scheme (4.73) can be applied by replacing material and conformation velocities, $\mathbf{v}$ and $\dot{\mathbf{a}}$, by their effective counterparts $\tilde{\mathbf{v}}$ and $\dot{\tilde{\mathbf{a}}}$:

$$\begin{cases} \mathbf{x}_{ij}(t) = \mathbf{x}_{ij}^0 + \int_{\tau=0}^{\tau=t} \tilde{\mathbf{v}}(\mathbf{x}_{ij}(\tau)) \, d\tau \\ \mathbf{a}_{ij}(t) = \mathbf{a}_{ij}^0 + \int_{\tau=0}^{\tau=t} \dot{\tilde{\mathbf{a}}}_{ij}(\mathbf{a}_{ij}(\tau), \mathbf{x}_{ij}(\tau)) \, d\tau \end{cases}. \tag{4.81}$$

This fully deterministic particle description requires much less particles that its stochastic counterpart, but as noticed in Eq. (4.80), the calculation of the effective material and conformational velocities requires the derivative of the pdf Ψ with respect to both the physical and the conformational coordinates. To do so, the distribution must be reconstructed all along the simulation (at each time step), which constitutes a serious drawback for its implementation on massively parallel computing platforms. Moreover, to make possible the calculation of the distribution derivatives, the Dirac distribution must be regularized in order to ensure its derivability.

4.3.2.2 Separated representations for solving difusion-dominated problems

When the diffusion effects are dominant, the techniques presented in the previous section become inefficient because they require an excessive number of particles to produce accurate enough results, in particular for reconstructing the distribution. In this case, standard mesh-based discretizations seem a better choice. However, as discussed before, mesh-based discretizations fail when addressing highly dimensional models as it is the case when addressing the solution of the previous introduced Fokker-Planck equation. Separated representations seem the most appealing choice.

Considering the Fokker-Planck equation

$$\frac{\partial \Psi}{\partial t} + \nabla_x \cdot (\mathbf{v} \, \Psi) + \nabla_a \cdot (\dot{\mathbf{a}} \, \Psi) = \nabla_x \left(\mathbf{D}_x \cdot \nabla_x \Psi \right) + \nabla_a \left(\mathbf{D}_a \cdot \nabla_a \Psi \right), \tag{4.82}$$

there are many separated representation choices. The most natural one consists in separating time, physical and conformational spaces, i.e.

$$\Psi(\mathbf{x}, t, \mathbf{a}) \approx \sum_{i=1}^{N} X_i(\mathbf{x}) \cdot T_i(t) \cdot A_i(\mathbf{a}). \tag{4.83}$$

Thus, when proceeding with the Proper Generalized Decomposition – PGD – constructor [4, 5, 19, 20], we must solve of the order of N 2D or 3D (depending on the dimension of the physical space) boundary value problems – BVP – for calculating functions $X_i(\mathbf{x})$, the same number of 1D initial value problems – IVP – for calculating functions $T_i(t)$, and finally the same number of problems involving the conformational coordinates for calculating functions $A_i(\mathbf{a})$.

4.3.3 Dilute suspensions of Brownian rods

In section 4.3.1 Brownian effects were neglected. The Brownian effects are due to the fluid molecules bombardment acting on the rod beads. This section focuses on the modeling of such effects particularly important when considering nano-charges (e.g. carbon nanotubes – CNT –). Moreover, as that bombardement results in a diffusion mechanism inducing a sort of randomizing effet, the same modeling framework is usually retained to address semi-dilute or semi-concentrated suspensions of rods in order to take into account the inter-rods interactions.

4.3.3.1 Microscopic description

In this case the rod beads are subjected to the hydrodynamic forces and the ones coming from the bombardment. The first one was introduced previously

$$\mathbf{F}^H = \xi L\,(\nabla \mathbf{v}\cdot\mathbf{p} - \dot{\mathbf{p}}), \tag{4.84}$$

where the superscript 'H" refers to its hydrodynamic nature. Now the Brownian force $\mathbf{F}^B$ is assumed to act during a short time interval δt following a certain statistical distribution concerning its magnitude and its orientation. The first one, in virtue of the central limit theorem, is assumed to be described by a gaussian distribution of zero mean and a certain standard deviation and the one related to the orientation by a uniform distribution on the unit circle $\mathscr{C}$ (in 2D) or in the unit sphere $\mathscr{S}$ (in 3D).

Brownian forces acting in the rod direction are assumed equilibrated. However, the components of those forces perpendicular to the rod axis contribute to the rod rotation, and then they affect its rotary velocity. In what follows, for the sake of clarity, we restrict our analysis to the 2D case. For inertialess rods the resultant moment must vanish and consequently

$$\mathbf{F}^H\cdot\mathbf{t} + \mathbf{F}^B\cdot\mathbf{t} = 0, \tag{4.85}$$

being $\mathbf{t}$ the unit vector tangent to the unit cercle defined from $\mathbf{t} = \frac{\dot{\mathbf{p}}}{\|\dot{\mathbf{p}}\|}$.

By injecting into Eq. (4.85) the hydrodynamic force (4.84) it results

$$\mathbf{t}^T\cdot\nabla\mathbf{v}\cdot\mathbf{p} - \|\dot{\mathbf{p}}\| = -\frac{\mathbf{F}^B\cdot\mathbf{t}}{\xi L}, \tag{4.86}$$

and multiplying by $\mathbf{t}$, taking into that $\dot{\mathbf{p}} = \|\dot{\mathbf{p}}\|\mathbf{t}$, it results

$$\dot{\mathbf{p}} = \left(\mathbf{t}^T \cdot \nabla \mathbf{v} \cdot \mathbf{p}\right)\mathbf{t} + \frac{\mathbf{F}^B \cdot \mathbf{t}}{\xi L}\,\mathbf{t}, \tag{4.87}$$

that using the vectorial equivalence

$$\left(\mathbf{t}^T \cdot \nabla \mathbf{v} \cdot \mathbf{p}\right)\mathbf{t} = \nabla \mathbf{v} \cdot \mathbf{p} - \left(\mathbf{p}^T \cdot \nabla \mathbf{v} \cdot \mathbf{p}\right)\mathbf{p}, \tag{4.88}$$

results in

$$\dot{\mathbf{p}} = \nabla \mathbf{v} \cdot \mathbf{p} - \left(\mathbf{p}^T \cdot \nabla \mathbf{v} \cdot \mathbf{p}\right)\mathbf{p} + \frac{\mathbf{F}^B \cdot \mathbf{t}}{\xi L}\,\mathbf{t} =$$

$$\nabla \mathbf{v} \cdot \mathbf{p} - \left(\mathbf{p}^T \cdot \nabla \mathbf{v} \cdot \mathbf{p}\right)\mathbf{p} + \frac{\mathbf{F}^B - (\mathbf{F}^B \cdot \mathbf{p})\mathbf{p}}{\xi L}, \tag{4.89}$$

where we can notice that the rotary velocity is given by the Jeffery expression $\dot{\mathbf{p}}^J$ complemented with a term accounting for the Bownian effects $\dot{\mathbf{p}}^B$,

$$\dot{\mathbf{p}}^J = \nabla \mathbf{v} \cdot \mathbf{p} - \left(\mathbf{p}^T \cdot \nabla \mathbf{v} \cdot \mathbf{p}\right)\mathbf{p}, \tag{4.90}$$

and

$$\dot{\mathbf{p}}^B = \frac{\mathbf{F}^B - (\mathbf{F}^B \cdot \mathbf{p})\mathbf{p}}{\xi L}, \tag{4.91}$$

from which

$$\dot{\mathbf{p}} = \dot{\mathbf{p}}^J + \dot{\mathbf{p}}^B. \tag{4.92}$$

Now, we discuss the effects of such Brownian contribution to the extra-stress tensor.

Consider a rod aligned along the x-axis, such that $\mathbf{p}^T = (1,0)$ and the fluid at rest. This rod undergone a continuous bombardment from the suspending fluid molecules. The component of forces aligned with the rod axis does not contribute to the rod rotation and by averaging it in $\Delta t \gg \delta t$ (Δt and δt being the rod kinematics characteristic time and the one related to the bombardement respectively) the resulting contribution vanishes. On the contrary, the component perpendicular to the rod will contribute to the stress. To derive the expression of this Brownian contribution we consider that due to an impact the rod rotates a small angle, e.g. $\delta\theta > 0$, with the rod orientation defined by $\mathbf{p}_{\delta\theta}$. We consider the unit tangent vector $\mathbf{t}_{\delta\theta}$ such that $\mathbf{p}_{\delta\theta} \times \mathbf{t}_{\delta\theta} = \mathbf{e}_z$ ($\mathbf{e}_z$ is the unit vector in the out-of-plane direction in the present 2D analysis). Considering the Brownian force applying at that position, i.e. $\|\mathbf{F}^B\| \cdot \mathbf{t}_{\delta\theta}$, it results the contribution to the virial stress

$$-\|\mathbf{F}^B\|\,\mathbf{p}_{\delta\theta} \otimes \mathbf{t}_{\delta\theta} = \|\mathbf{F}^B\| \begin{pmatrix} \sin(\delta\theta)\,\cos(\delta\theta) & -\cos^2(\delta\theta) \\ \sin^2(\delta\theta) & -\sin(\delta\theta)\,\cos(\delta\theta) \end{pmatrix}, \tag{4.93}$$

where the negative sign accounts for the fact that the hydrodynamic force applies in the opposite direction of the Brownian force.

We can notice in that expression two facts: (i) the trace is zero, and (ii) the contribution is non-symmetric. However, we can imagine that a little bit later, a Brownian force will apply in the opposite direction. Invoking ergodicity (allowing to replace time by ensemble averages) we could assume that another particle initially aligned along $\mathbf{p}$ receive the opposite impact leading to an angle $-\delta\theta$, from which

$$\|\mathbf{F}^B\|\ \mathbf{p}_{-\delta\theta}\otimes\mathbf{t}_{-\delta\theta} = \|\mathbf{F}^B\|\ \begin{pmatrix} \sin(\delta\theta)\ \cos(\delta\theta) & \cos^2(\delta\theta) \\ -\sin^2(\delta\theta) & -\sin(\delta\theta)\ \cos(\delta\theta) \end{pmatrix}, \tag{4.94}$$

and then by averaging it gives a Brownian contribution to the extra-stress associated to the x-direction ($\varphi = 0$)

$$\tau^B_{\varphi=0} = \begin{pmatrix} \beta & 0 \\ 0 & -\beta \end{pmatrix} = \beta \begin{pmatrix} 1 & 0 \\ 0 & -1 \end{pmatrix} = \beta\ \mathbf{U}, \tag{4.95}$$

that becomes symmetric and traceless.

Now, for rods aligned in any other direction φ, it suffices to apply a rotation of angle φ to tensor $\tau^B_{\varphi=0}$ according to

$$\tau^B_\varphi = \beta\ \mathbf{R}^T_\varphi \cdot \mathbf{U} \cdot \mathbf{R}_\varphi, \tag{4.96}$$

with

$$\mathbf{R}_\varphi = \begin{pmatrix} \cos\varphi & \sin\varphi \\ -\sin\varphi\ \cos\varphi \end{pmatrix}, \tag{4.97}$$

that finally yields

$$\tau^B_\varphi = 2\beta\ \left(\begin{pmatrix} \cos^2\varphi & \sin\varphi\ \cos\varphi \\ \sin\varphi\ \cos\varphi & \sin^2\varphi \end{pmatrix} - \begin{pmatrix} \frac{1}{2} & 0 \\ 0 & \frac{1}{2} \end{pmatrix} \right), \tag{4.98}$$

that can be rewritten as

$$\tau^B_{\mathbf{p}_\varphi} = 2\beta\ \left(\mathbf{p}_\varphi \otimes \mathbf{p}_\varphi - \frac{\mathbf{I}}{2} \right), \tag{4.99}$$

where $\mathbf{I}$ is the identity tensor and $\mathbf{p}_\varphi$ the unit vector defined by the angle φ.

For a population of rods $\mathbf{p}_i$, $i = 1, \cdots, N$, the contribution of Brownian effects is finally given by:

$$\tau^B = 2\beta\ \sum_{i=1}^{N} \left(\mathbf{p}_i \otimes \mathbf{p}_i - \frac{\mathbf{I}}{2} \right). \tag{4.100}$$

4.3.3.2 Mesoscopic description

The mesoscopic discrete description can be summarized as follows:

- Given the flow velocity field $\mathbf{v}(\mathbf{x}, t)$, the initial position of the centre of gravity of each rod $\mathbf{x}^G_i(t=0)$ and its orientation $\mathbf{p}_i(t=0)$ or knowing both them at time t;

- For each rod $i = 1, \cdots, N$:
  - Update the position of the centre of gravity by integrating:

$$\frac{d\mathbf{x}_i^G}{dt} = \mathbf{v}(\mathbf{x}_i^G, t). \tag{4.101}$$

  - Update its orientation by integrating

$$\frac{d\mathbf{p}_i}{dt} = \nabla \mathbf{v}|_{\mathbf{x}_i^G,t} \cdot \mathbf{p}_i - \left(\mathbf{p}_i^T \cdot \nabla \mathbf{v}|_{\mathbf{x}_i^G,t} \cdot \mathbf{p}_i\right)\ \mathbf{p}_i + \frac{\mathbf{F}_i^B - (\mathbf{F}_i^B \cdot \mathbf{p}_i)\ \mathbf{p}_i}{\xi L}. \tag{4.102}$$

- Compute the stress at position $\mathbf{x}$ and time t by considering all the rods inside a control volume $\mathscr{V}(\mathbf{x})$ centered at $\mathbf{x}$ by applying

$$\tau(\mathbf{x},t) = 2\eta\ \mathbf{D}(\mathbf{x},t) +$$

$$+ \sum_{i \in \mathscr{V}(\mathbf{x})} \left(2\eta N_p\ \nabla \mathbf{v}|_{\mathbf{x},t} : (\mathbf{p}_i \otimes \mathbf{p}_i \otimes \mathbf{p}_i \otimes \mathbf{p}_i) + 2\beta\ \left(\mathbf{p}_i \otimes \mathbf{p}_i - \frac{\mathbf{I}}{2}\right)\right). \tag{4.103}$$

  In the case of coupled models this stress will serve to update the velocity field, however, as previously indicated, in the present text we consider the velocity field unperturbed by the presence and orientation of the rods (decoupled modeling).

On the other hand the mesoscopic continuous description considers a diffusion term in the Fokker-Planck equation

$$\frac{\partial \Psi}{\partial t} + \nabla_x \cdot (\mathbf{v}\Psi) + \nabla_p \cdot (\dot{\mathbf{p}}\Psi) = D_r \nabla_p^2 \Psi, \tag{4.104}$$

with the flow induced orientation $\dot{\mathbf{p}}$ given by the Jeffery's equation (4.49), and where D_r is the so-called rotary diffusion.

We can notice that in absence of flow, i.e. $\mathbf{v}(\mathbf{x},t) = \mathbf{0}$ the Fokker-Planck equation reduces to

$$\frac{\partial \Psi}{\partial t} = D_r \nabla_p^2 \Psi, \tag{4.105}$$

that ensures a steady state consisting of an isotropic orientation distribution, i.e. $\Psi(\mathbf{x}, t \to \infty, \mathbf{p}) = \frac{1}{2\pi}$ in 2D and $\Psi(\mathbf{x}, t \to \infty, \mathbf{p}) = \frac{1}{4\pi}$ in 3D. The higher is the rotational diffusion the faster the isotropic orientation distribution is reached.

Thus, at the continuous mesoscopic level the introduction of Brownian effects seems quite simple. The question is: what is the discrete and macroscopic counterparts of the just introduced diffusion term?

The Fokker-Planck equation can be rewritten in the form:

$$\frac{\partial \Psi}{\partial t} + \nabla_x \cdot (\mathbf{v}\Psi) + \nabla_p \cdot (\dot{\mathbf{p}}\Psi) - D_r \nabla_p^2 \Psi =$$

$$\frac{\partial \Psi}{\partial t} + \nabla_x \cdot (\mathbf{v}\Psi) + \nabla_p \cdot \left(\dot{\tilde{\mathbf{p}}}\Psi\right) = 0, \tag{4.106}$$

where the effective rotational velocity $\dot{\tilde{\mathbf{p}}}$ is given by

$$\dot{\tilde{\mathbf{p}}} = \nabla \mathbf{v} \cdot \mathbf{p} - \left(\mathbf{p}^T \cdot \nabla \mathbf{v} \cdot \mathbf{p}\right) \mathbf{p} - D_r \frac{\nabla_p \Psi}{\Psi} \tag{4.107}$$

that contains the flow induced Jeffery's contribution $\dot{\mathbf{p}}^J$ plus the Brownian one $\dot{\mathbf{p}}^B$, i.e. $\dot{\tilde{\mathbf{p}}} = \dot{\mathbf{p}}^J + \dot{\mathbf{p}}^B$ with

$$\dot{\mathbf{p}}^J = \nabla \mathbf{v} \cdot \mathbf{p} - \left(\mathbf{p}^T \cdot \nabla \mathbf{v} \cdot \mathbf{p}\right) \mathbf{p}, \tag{4.108}$$

and

$$\dot{\mathbf{p}}^B = -D_r \frac{\nabla_p \Psi}{\Psi}. \tag{4.109}$$

Within the mesoscopic continuous description Brownian contribution to the extra-stress tensor results from the generalization of Eq. (4.100) by substituting the sum by that corresponding integral

$$\tau^B = 2\tilde{\beta} \int_{\mathscr{S}} \left(\mathbf{p} \otimes \mathbf{p} - \frac{\mathbf{I}}{2}\right) \Psi(\mathbf{p}) \, d\mathbf{p} = 2\tilde{\beta} \left(\mathbf{a} - \frac{\mathbf{I}}{2}\right). \tag{4.110}$$

In summary, the mesoscopic continuous description consists of:

- Given the flow velocity field $\mathbf{v}(\mathbf{x}, t)$ and the initial orientation distribution $\Psi(\mathbf{x}, t = 0, \mathbf{p})$
- Solve the Fokker-Planck equation that governs the rods orientation distribution:

$$\frac{\partial \Psi}{\partial t} + \nabla_x \cdot (\mathbf{v}\Psi) + \nabla_p \cdot (\dot{\mathbf{p}}\Psi) = D_r \nabla_p^2 \Psi, \tag{4.111}$$

  with

$$\dot{\mathbf{p}} = \nabla \mathbf{v} \cdot \mathbf{p} - \left(\mathbf{p}^T \cdot \nabla \mathbf{v} \cdot \mathbf{p}\right) \mathbf{p}. \tag{4.112}$$

- Compute the stress tensor:

$$\tau = \tau^f + \tau^r = 2\eta \, \mathbf{D} + 2\eta N_p \, (\mathbf{D} : \mathbf{A}) + 2\tilde{\beta} \left(\mathbf{a} - \frac{\mathbf{I}}{2}\right). \tag{4.113}$$

4.3.3.3 Macroscopic description

When moving towards the macroscopic scale the Brownian contribution to the extra-stress is defined by Eq. (4.110), however at the macroscopic scale the microstructure is defined by the different moments of the orientation distribution. In what follows we are deriving the contribution of Brownian effects on the equation governing the evolution of the second order moment.

We start from the second order moment definition

$$\mathbf{a} = \int_{\mathscr{S}} \mathbf{p} \otimes \mathbf{p} \, \Psi \, d\mathbf{p} \tag{4.114}$$

whose time derivative involves now the effective rotational velocity $\dot{\tilde{\mathbf{p}}}$

$$\dot{\mathbf{a}} = \int_{\mathscr{S}} \left(\dot{\tilde{\mathbf{p}}} \otimes \mathbf{p} + \mathbf{p} \otimes \dot{\tilde{\mathbf{p}}} \right) \Psi \, d\mathbf{p}. \tag{4.115}$$

As proved in the previous sections, the effective rotational velocity contains the flow induced contribution given by the Jeffery's expression $\dot{\mathbf{p}}^J$ and the one induced by the Brownian effects $\dot{\mathbf{p}}^B$, given by Eqs. (4.108) and (4.109) respectively. With this decomposition Eq. (4.115) can be written as

$$\begin{aligned} \dot{\mathbf{a}} = \int_{\mathscr{S}} \left(\left(\dot{\mathbf{p}}^J + \dot{\mathbf{p}}^B \right) \otimes \mathbf{p} + \mathbf{p} \otimes \left(\dot{\mathbf{p}}^J + \dot{\mathbf{p}}^B \right) \right) \, \Psi \, d\mathbf{p} = \\ \int_{\mathscr{S}} \left(\dot{\mathbf{p}}^J \otimes \mathbf{p} + \mathbf{p} \otimes \dot{\mathbf{p}}^J \right) \, \Psi \, d\mathbf{p} + \\ \int_{\mathscr{S}} \left(\dot{\mathbf{p}}^B \otimes \mathbf{p} + \mathbf{p} \otimes \dot{\mathbf{p}}^B \right) \, \Psi \, d\mathbf{p} = \dot{\mathbf{a}}^J + \dot{\mathbf{a}}^B, \end{aligned} \tag{4.116}$$

where the flow induced microstructure evolution $\dot{\mathbf{a}}^J$ is given by

$$\dot{\mathbf{a}}^J = \nabla \mathbf{v} \cdot \mathbf{a} + \mathbf{a} \cdot (\nabla \mathbf{v})^T - 2\mathbf{A} : \mathbf{D}. \tag{4.117}$$

We are now calculating the expression of the remaining contribution $\dot{\mathbf{a}}^B$

$$\dot{\mathbf{a}}^B = \int_{\mathscr{S}} \left(\dot{\mathbf{p}}^B \otimes \mathbf{p} + \mathbf{p} \otimes \dot{\mathbf{p}}^B \right) \Psi \, d\mathbf{p}, \tag{4.118}$$

with $\dot{\mathbf{p}}^B$ given by

$$\dot{\mathbf{p}}^B = -D_r \frac{\nabla_p \Psi}{\Psi}. \tag{4.119}$$

For the sake of clarity we consider again the 2D case that allows to write

$$\dot{\mathbf{p}}^B = -D_r \frac{\| \nabla_p \Psi \|}{\Psi} \, \mathbf{t}, \tag{4.120}$$

with $\mathbf{t}$ being the unit tangent vector to the unit circle aligned with the rotary velocity. In this case Eq. (4.118) reduces to

$$\dot{\mathbf{a}}^B = -D_r \int_{\mathscr{S}} \left(\mathbf{t} \otimes \mathbf{p} + \mathbf{p} \otimes \mathbf{t} \right) \, \frac{\partial \Psi}{\partial \theta} \, d\theta. \tag{4.121}$$

Now, integrating by parts Eq. (4.121) and taking into account

$$\frac{d\mathbf{p}}{d\theta} = \mathbf{t}, \tag{4.122}$$

and

$$\frac{d\mathbf{t}}{d\theta} = -\mathbf{p}, \tag{4.123}$$

it results that

$$\dot{\mathbf{a}}^B = -2D_r \int_{\mathscr{S}} (\mathbf{p}\otimes\mathbf{p} - \mathbf{t}\otimes\mathbf{t})\ \Psi(\theta)\ d\theta. \tag{4.124}$$

It is easy to prove that

$$\mathbf{t}\otimes\mathbf{t} + \mathbf{p}\otimes\mathbf{p} = \mathbf{I} \ \rightarrow\ \mathbf{t}\otimes\mathbf{t} = \mathbf{I} - \mathbf{p}\otimes\mathbf{p}, \tag{4.125}$$

that allows to write Eq. (4.124) in the form

$$\dot{\mathbf{a}}^B = -2D_r \int_{\mathscr{S}} (2(\mathbf{p}\otimes\mathbf{p}) - \mathbf{I})\ \Psi(\theta)\ d\theta = -2D_r\,(2\mathbf{a} - \mathbf{I}) \tag{4.126}$$

or

$$\dot{\mathbf{a}}^B = -4D_r \left(\mathbf{a} - \frac{\mathbf{I}}{2}\right). \tag{4.127}$$

When considering a 3D situation, the resulting expression is given by

$$\dot{\mathbf{a}}^B = -6D_r \left(\mathbf{a} - \frac{\mathbf{I}}{3}\right). \tag{4.128}$$

We can notice that in the 2D case and in absence of flow, $\dot{\mathbf{a}}^J = \mathbf{0}$, and then $\dot{\mathbf{a}} = \dot{\mathbf{a}}^B$

$$\dot{\mathbf{a}} = -4D_r \left(\mathbf{a} - \frac{\mathbf{I}}{2}\right), \tag{4.129}$$

ensuring an isotropic steady state, i.e. $\mathbf{a}(t\rightarrow\infty) = \frac{\mathbf{I}}{2}$.

In summary, the decoupled macroscopic description consists of:

- Given the flow velocity field $\mathbf{v}(\mathbf{x},t)$ and the initial second order moment of the orientation distribution $\mathbf{a}(\mathbf{x},t=0)$;
- Solve the equation governing the evolution of $\mathbf{a}$:

$$\dot{\mathbf{a}} = \nabla\mathbf{v}\cdot\mathbf{a} + \mathbf{a}\cdot(\nabla\mathbf{v})^T - 2\mathbf{A}:\mathbf{D} - 4D_r\left(\mathbf{a} - \frac{\mathbf{I}}{2}\right), \ \text{in 2D}, \tag{4.130}$$

  by using an exact or an approximated closure relation.
- Compute the stress tensor:

$$\tau = \tau^f + \tau^r = 2\eta\mathbf{D} + 2\eta N_p\,(\mathbf{D}:\mathbf{A}) + 2\tilde{\beta}\left(\mathbf{a} - \frac{\mathbf{I}}{2}\right), \ \text{in 2D}, \tag{4.131}$$

  using again an appropriate closure relation.

4.3.3.4 From semi-dilute to concentrated regimes

Semi-dilute and semi-concentrated regimes have been widely addressed, most of time by using phenomenological approaches. The most common approach consists

in considering that rod-rod interactions tends to randomize the orientation distribution. Thus, a second diffusion coefficient is introduced for accounting for rods interactions, however, in the present case that diffusion coefficient should scale with the flow intensity in order to ensure that in absence of flow the microstructure does not evolve artificially due to such a diffusion term. In general the interaction diffusion coefficient D_I is assumed in the general form

$$D_I = C_I \, f(D^{eq}) \tag{4.132}$$

where D^{eq} is related to the second invariant of the rate of strain tensor, i.e. $D^{eq} = \sqrt{\mathbf{D} : \mathbf{D}}$ and C_I is the so-called interaction coefficient. The Folgar & Tucker model considers the simplest dependence $f(D^{eq}) = D^{eq}$.

Obviously, there are finer approaches based on the direct simulation where the rod-rod interactions are taken explicitly into account. In the concentrated regime the subjacent physics is richer and many times it involves aggregation. The interested reader can refer to chapter 2 in [12] and the references therein.

4.3.4 Rigid clusters composed of rigid rods

The kinematics of rigid and deformable clusters composed of rods was widely described in [12]. When focusing on rigid clusters it was assumed that hydrodynamic forces (previously introduced) act on the N beads of the rods involved in the cluster. The location of each bead $\mathscr{B}_i$ with respect to the cluster center of gravity $\mathbf{G}$ is given by $L_i\mathbf{p}_i$, where $\mathbf{p}_i$ is the unit vector pointing from $\mathbf{G}$ to $\mathscr{B}_i$, as shown in Fig. 4.3.

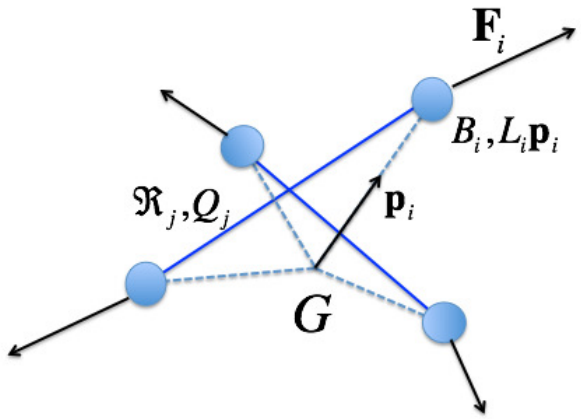

Fig. 4.3 Rigid cluster composed of rods.

A balance of torques yields the cluster rotary velocity. By defining the cluster conformation tensor $\mathbf{c}$ as follows,

$$\mathbf{c} = \frac{\sum_{i=1}^{N} L_i^2 \, (\mathbf{p}_i \otimes \mathbf{p}_i)}{\sum_{i=1}^{N} L_i^2}, \tag{4.133}$$

the cluster rotary velocity ω is given by

$$\omega = (\mathbf{I} - \mathbf{c})^{-1} (\varepsilon : (\nabla \mathbf{v} \cdot \mathbf{c})), \tag{4.134}$$

where ε the Levi-Civita permutation tensor. From the cluster rotary velocity ω given by Eq. (4.134), the rate of change of the conformation tensor $\dot{\mathbf{c}}$ can be calculated [2, 12].

Thus, different cluster having the same conformation tensor $\mathbf{c}$ will have the same rotary velocity. A particular case consists of the tri-dumbell whose rotary velocity calculated from the previous equations coincides with the one associated to the Jeffery solution for the corresponding ellipsoid. In the next section 4.3.4.1 we describe the rationale in the case of a rigid bi-dumbbell.

In the limit case when the number of rods is large enough, the discrete description given by Eq. (4.133) can be substituted by a continuous one that considers the pdf $\psi(\mathbf{p})$ given the fraction of rods in the cluster aligned in direction $\mathbf{p}$.

A dilute suspension composed of rigid clusters could be described within the kinetic theory framework by using a second pdf, the one related to the clusters distributed in the suspending medium, $\Psi(\mathbf{x}, t, \mathbf{c})$, given the fraction of cluster that at position $\mathbf{x}$ and time t have a conformation $\mathbf{c}$. Being the conformation tensor $\mathbf{c}$ symmetric and with unit trace, it has in the general 3D case 5 independent components, that is 5 conformational coordinates. The associated Fokker-Planck equation reads

$$\frac{\partial \Psi}{\partial t} + \nabla_x \cdot (\mathbf{v}\Psi) + \nabla_c \cdot (\dot{\mathbf{c}}\Psi) = 0, \tag{4.135}$$

whose high dimensionality compromises the use of standard mesh-based discretization techniques for solving it, as discussed in [1].

4.3.4.1 Orthogonal rigid bi-dumbbell: Revisiting general Jeffery's equation

In what follows we first prove that the kinematics of a rigid ellipse immersed in a flow can be obtained from the analysis of a rigid bi-dumbbell. The Jeffery's equation for an ellipse of aspect ratio r (major to minor axes ratio) when considering the decomposition of the velocity gradient in its symmetric (the rate of strain tensor $\mathbf{D}$) and skew-symmetric component (the vorticity tensor Ω), $\nabla \mathbf{v} = \mathbf{D} + \Omega$ reads

$$\dot{\mathbf{p}} = \Omega \cdot \mathbf{p} + \mathscr{F}(\mathbf{D} \cdot \mathbf{p} - (\mathbf{p}^T \cdot \mathbf{D} \cdot \mathbf{p})\mathbf{p}), \tag{4.136}$$

with the shape factor $\mathscr{F} = \frac{r^2-1}{r^2+1}$.

In what follows we consider a rigid system composed of two rods, mutually perpendicular, and having respectively length $2L_1$ and $2L_2$ ($L_1 > L_2$) as sketched in Fig. 4.4.

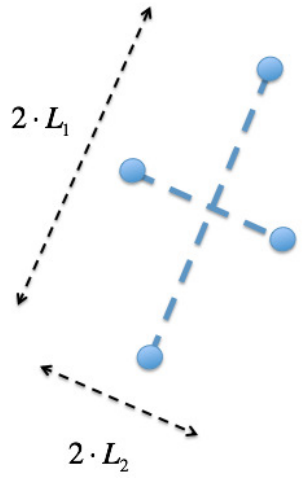

Fig. 4.4 Two-rods rigid cluster representing an elliptic 2D particle

In the present configuration the hydrodynamic forces acting in bead $L_1\mathbf{p}_1$ and $L_2\mathbf{p}_2$, $\mathbf{F}_1^H$ and $\mathbf{F}_2^H$ respectively read

$$\mathbf{F}_1^H = \xi L_1(\nabla\mathbf{v}\cdot\mathbf{p}_1 - \dot{\mathbf{p}}_1), \tag{4.137}$$

and

$$\mathbf{F}_2^H = \xi L_2(\nabla\mathbf{v}\cdot\mathbf{p}_2 - \dot{\mathbf{p}}_2), \tag{4.138}$$

with $\mathbf{p}_1 \perp \mathbf{p}_2$, and with their rates of change expressed from

$$\begin{cases} \dot{\mathbf{p}}_1 = \boldsymbol{\omega}\times\mathbf{p}_1 \\ \dot{\mathbf{p}}_2 = \boldsymbol{\omega}\times\mathbf{p}_2 \end{cases}, \tag{4.139}$$

where $\boldsymbol{\omega}$ denotes the angular velocity.

The angular momentum balance implies

$$L_1^2\mathbf{p}_1\times(\nabla\mathbf{v}\cdot\mathbf{p}_1 - \dot{\mathbf{p}}_1) + L_2^2\mathbf{p}_2\times(\nabla\mathbf{v}\cdot\mathbf{p}_2 - \dot{\mathbf{p}}_2) = \mathbf{0}. \tag{4.140}$$

Introducing (4.139) into (4.140) and taking into account that $\mathbf{p}_1\times\boldsymbol{\omega}\times\mathbf{p}_1 = \boldsymbol{\omega}$ and $\mathbf{p}_2\times\boldsymbol{\omega}\times\mathbf{p}_2 = \boldsymbol{\omega}$, it results that

$$\boldsymbol{\omega} = \frac{L_1^2}{L_1^2+L_2^2}\left(\mathbf{p}_1\times(\nabla\mathbf{v}\cdot\mathbf{p}_1)\right) + \frac{L_2^2}{L_1^2+L_2^2}\left(\mathbf{p}_2\times(\nabla\mathbf{v}\cdot\mathbf{p}_2)\right). \tag{4.141}$$

Thus, $\dot{\mathbf{p}}_1$ can be expressed from

$$\dot{\mathbf{p}}_1 = \omega \times \mathbf{p}_1 =$$

$$\frac{L_1^2}{L_1^2+L_2^2}\left((\mathbf{p}_1 \times (\nabla \mathbf{v} \cdot \mathbf{p}_1)) \times \mathbf{p}_1\right) + \frac{L_2^2}{L_1^2+L_2^2}\left((\mathbf{p}_2 \times (\nabla \mathbf{v} \cdot \mathbf{p}_2) \times \mathbf{p}_1)\right). \tag{4.142}$$

Now, applying the triple vector product formula $(\mathbf{a}\times\mathbf{b})\times\mathbf{c} = -\mathbf{a}\cdot(\mathbf{b}\cdot\mathbf{c}) + \mathbf{b}\cdot(\mathbf{a}\cdot\mathbf{c})$, Eq. (4.142) reads

$$\dot{\mathbf{p}}_1 = \frac{L_1^2}{L_1^2+L_2^2}\left(\nabla \mathbf{v} \cdot \mathbf{p}_1 - \left(\mathbf{p}_1^T \cdot \nabla \mathbf{v} \cdot \mathbf{p}_1\right)\mathbf{p}_1\right) -$$

$$\frac{L_2^2}{L_1^2+L_2^2}\left(\left(\mathbf{p}_1^T \cdot \nabla \mathbf{v} \cdot \mathbf{p}_2\right)\mathbf{p}_2\right). \tag{4.143}$$

We are developing the last term in Eq. (4.143) to obtain an equation that only contains $\mathbf{p}_1$ in order to compare with the Jeffery's one. First we apply the decomposition $\nabla\mathbf{v} = \mathbf{D} + \Omega$ from which the last term in Eq. (4.143) reads

$$\left(\mathbf{p}_1^T \cdot \nabla \mathbf{v} \cdot \mathbf{p}_2\right)\mathbf{p}_2 = \left(\mathbf{p}_1^T \cdot \mathbf{D} \cdot \mathbf{p}_2\right)\mathbf{p}_2 + \left(\mathbf{p}_1^T \cdot \Omega \cdot \mathbf{p}_2\right)\mathbf{p}_2, \tag{4.144}$$

where the first term in the right hand member, using the fact that $\mathbf{D}$ is symmetric, reads

$$\left(\mathbf{p}_1^T \cdot \mathbf{D} \cdot \mathbf{p}_2\right)\mathbf{p}_2 =$$

$$\mathbf{p}_2\left(\mathbf{p}_1^T \cdot \mathbf{D} \cdot \mathbf{p}_2\right) = \mathbf{p}_2\left(\mathbf{p}_2^T \cdot \mathbf{D} \cdot \mathbf{p}_1\right) = (\mathbf{p}_2 \otimes \mathbf{p}_2) \cdot \mathbf{D} \cdot \mathbf{p}_1. \tag{4.145}$$

Now, using the orthogonality of $\mathbf{p}_1$ and $\mathbf{p}_2$, it results that

$$(\mathbf{p}_2 \otimes \mathbf{p}_2) + (\mathbf{p}_1 \otimes \mathbf{p}_1) = \mathbf{I}, \tag{4.146}$$

and then Eq. (4.145) can be written as

$$\left(\mathbf{p}_1^T \cdot \mathbf{D} \cdot \mathbf{p}_2\right)\mathbf{p}_2 = (\mathbf{I} - \mathbf{p}_1 \otimes \mathbf{p}_1) \cdot \mathbf{D} \cdot \mathbf{p}_1. \tag{4.147}$$

Finally we consider the second term in the right-hand side of Eq. (4.144), using the fact that Ω is skew-symmetric

$$\left(\mathbf{p}_1^T \cdot \Omega \cdot \mathbf{p}_2\right)\mathbf{p}_2 =$$

$$\mathbf{p}_2\left(\mathbf{p}_1^T \cdot \Omega \cdot \mathbf{p}_2\right) = -\mathbf{p}_2\left(\mathbf{p}_2^T \cdot \Omega \cdot \mathbf{p}_1\right) = -(\mathbf{p}_2 \otimes \mathbf{p}_2) \cdot \Omega \cdot \mathbf{p}_1, \tag{4.148}$$

that is

$$\left(\mathbf{p}_1^T \cdot \Omega \cdot \mathbf{p}_2\right)\mathbf{p}_2 = -(\mathbf{I} - \mathbf{p}_1 \otimes \mathbf{p}_1) \cdot \Omega \cdot \mathbf{p}_1. \tag{4.149}$$

Now, coming back to Eq. (4.143), we obtain

$$\dot{\mathbf{p}}_1 = \Omega \cdot \mathbf{p}_1 + \frac{L_1^2 - L_2^2}{L_1^2 + L_2^2} \mathbf{D} \cdot \mathbf{p}_1 - \frac{L_1^2 - L_2^2}{L_1^2 + L_2^2} \left(\mathbf{p}_1^T \cdot \mathbf{D} \cdot \mathbf{p}_1 \right) \mathbf{p}_1, \tag{4.150}$$

that corresponds exactly to the Jeffery expression for an ellipse of aspect ratio $\frac{L_1}{L_2}$.

4.3.5 Extensible rods

We consider the kinematics of an extensible rod, whose reference length is $2L^0$. In first gradient flows (at the rod scale) only rod extension and its rotation are activated by the flow kinematics. At time t, the rod, aligned in the direction $\mathbf{p}$, is represented by an elastic spring of length $2L$ and rigidity $\mathscr{K}$ equipped of two beads at its extremities where the hydrodynamic forces act. As previously considered the hydrodynamic force scales with the fluid/bead relative velocity, the former given by $\mathbf{v}_0 + \nabla \mathbf{v} \cdot \mathbf{p}L$ and the latter by $\mathbf{v}_G + \dot{\mathbf{p}}L + \mathbf{p}\dot{L}$, where $\mathbf{v}_0$ is the unperturbed fluid velocity at the rod center of gravity and $\mathbf{v}_G$ the velocity of the rod centre of gravity. A sketch of the elastic rod and the forces applying on it is depicted in Fig. 4.5

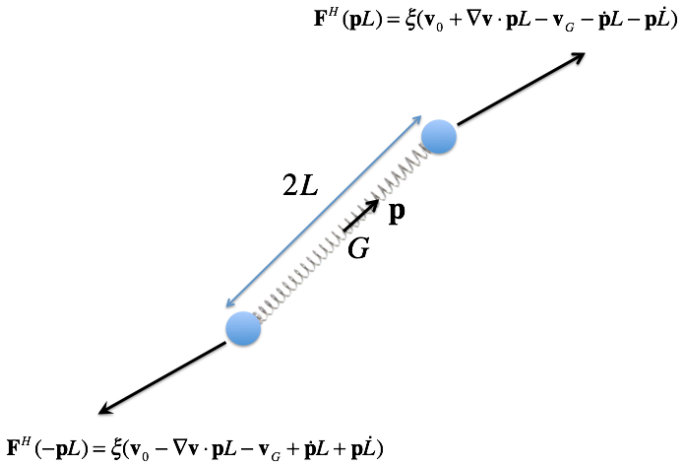

Fig. 4.5 Extensible fiber immersed in a flow.

The system is assumed inertialess, implying that the equilibrium of forces and torques should vanish. The first reads $\mathbf{F}^H(\mathbf{p}L) + \mathbf{F}^H(-\mathbf{p}L) = \mathbf{0}$, that implies $\mathbf{v}_0 = \mathbf{v}_G$, that is, the rod centre of gravity moves with the fluid.

Now, to prevent a resultant torque, force $\mathbf{F}^H(\mathbf{p}L)$ must align with $\mathbf{p}$, i.e. $\mathbf{F}^H(\mathbf{p}L) = \lambda\mathbf{p}$, $\lambda \in \mathbb{R}$. Thus, it results that

$$\mathbf{F}^H(\mathbf{p}L) = \xi(\nabla\mathbf{v} \cdot \mathbf{p}L - \dot{\mathbf{p}}L - \mathbf{p}\dot{L}) = \lambda\mathbf{p}, \tag{4.151}$$

that multiplying by $\mathbf{p}$ and taking into account that $\mathbf{p}\cdot\mathbf{p}=1$ and consequently $\mathbf{p}\cdot\dot{\mathbf{p}}=0$, yields

$$\xi(\nabla\mathbf{v}:(\mathbf{p}\otimes\mathbf{p})L-\dot{L})=\lambda. \tag{4.152}$$

Introducing this expression into Eq. (4.151) reads

$$\xi(\nabla\mathbf{v}\cdot\mathbf{p}L-\dot{\mathbf{p}}L-\mathbf{p}\dot{L})=\xi(\nabla\mathbf{v}:(\mathbf{p}\otimes\mathbf{p})L-\dot{L})\mathbf{p}, \tag{4.153}$$

and grouping terms

$$\dot{\mathbf{p}}=\nabla\mathbf{v}\cdot\mathbf{p}-\nabla\mathbf{v}:(\mathbf{p}\otimes\mathbf{p})\mathbf{p}, \tag{4.154}$$

that is nothing else than the standard Jeffery's expression for ellipsoids of infinite aspect ratio (rods) widely discussed in the previous sections.

Now by equating the force acting on the beads, λ, with the one installed in the spring, it results that

$$2\mathscr{K}(L-L^0)=\xi(\nabla\mathbf{v}:(\mathbf{p}\otimes\mathbf{p})L-\dot{L}), \tag{4.155}$$

or

$$\dot{L}=-\frac{2\mathscr{K}}{\xi}(L-L^0)+\nabla\mathbf{v}:(\mathbf{p}\otimes\mathbf{p})L. \tag{4.156}$$

Thus, the kinematics of an elastic dumbbell of reference length $2L^0$ immersed in a first gradient flow and described by its orientation $\mathbf{p}$ and length $2L$ is given by

$$\begin{cases}\dot{\mathbf{p}}=\nabla\mathbf{v}\cdot\mathbf{p}-\nabla\mathbf{v}:(\mathbf{p}\otimes\mathbf{p})\mathbf{p}\\ \dot{L}=-\frac{2\mathscr{K}}{\xi}(L-L^0)+\nabla\mathbf{v}:(\mathbf{p}\otimes\mathbf{p})L\end{cases}. \tag{4.157}$$

Before closing this section we address the case of a deformable bi-dumbbell that will be used later for deriving a micro-mechanical model of flowing foams.

4.3.5.1 Orthogonal elastic bi-dumbell

In the present configuration, and considering that as proven before the centre of gravity moves with the fluid, the hydrodynamic forces acting in bead $L_1\mathbf{p}_1$ and $L_2\mathbf{p}_2$, $\mathbf{F}_1^H$ and $\mathbf{F}_2^H$ respectively read

$$\mathbf{F}_1^H=\xi(\nabla\mathbf{v}\cdot\mathbf{p}_1L_1-\dot{\mathbf{p}}_1L_1-\mathbf{p}_1\dot{L}_1), \tag{4.158}$$

and

$$\mathbf{F}_2^H=\xi(\nabla\mathbf{v}\cdot\mathbf{p}_2L_2-\dot{\mathbf{p}}_2L_2-\mathbf{p}_2\dot{L}_2), \tag{4.159}$$

with again $\mathbf{p}_1\perp\mathbf{p}_2$, and with their rates of change expressed from

$$\begin{cases}\dot{\mathbf{p}}_1=\omega\times\mathbf{p}_1\\ \dot{\mathbf{p}}_2=\omega\times\mathbf{p}_2\end{cases}. \tag{4.160}$$

The angular momentum balance implies now

$$L_1^2\mathbf{p}_1\times(\nabla\mathbf{v}\cdot\mathbf{p}_1-\dot{\mathbf{p}}_1)+L_2^2\mathbf{p}_2\times(\nabla\mathbf{v}\cdot\mathbf{p}_2-\dot{\mathbf{p}}_2)=\mathbf{0}, \tag{4.161}$$

that coincides with the expression obtained in the case of orthogonal rigid bi-dumbbells, proving the validity of Jeffery equation in the case of orthogonal elastic bi-dumbell.

However, in the present case we need extra-equations giving the spring extensions $\dot{L}_1$ and $\dot{L}_2$. For that purpose we consider the Jeffery's equation (4.136) with $\mathscr{F}=\frac{L_1^2-L_2^2}{L_1^2+L_2^2}$, i.e.

$$\dot{\mathbf{p}}_1=\Omega\cdot\mathbf{p}_1+\mathscr{F}\left(\mathbf{D}\cdot\mathbf{p}_1-\left(\mathbf{p}_1^T\cdot\mathbf{D}\cdot\mathbf{p}_1\right)\mathbf{p}_1\right), \tag{4.162}$$

and introduce it into the expression of the hydrodynamic force acting on bead $\mathbf{p}_1L_1$ (4.158)

$$\begin{aligned}\mathbf{F}_1^H&=\xi(\nabla\mathbf{v}\cdot\mathbf{p}_1L_1-\dot{\mathbf{p}}_1L_1-\mathbf{p}_1\dot{L}_1)=\\ &\xi\left(\nabla\mathbf{v}\cdot\mathbf{p}_1L_1-\Omega\cdot\mathbf{p}_1L_1-\mathscr{F}\left(\mathbf{D}\cdot\mathbf{p}_1L_1-\left(\mathbf{p}_1^T\cdot\mathbf{D}\cdot\mathbf{p}_1\right)\mathbf{p}_1L_1\right)-\mathbf{p}_1\dot{L}_1\right)=\\ &\xi L_1\left((1-\mathscr{F})\mathbf{D}\cdot\mathbf{p}_1+\mathscr{F}\left(\mathbf{p}_1^T\cdot\mathbf{D}\cdot\mathbf{p}_1\right)\mathbf{p}_1\right)-\xi\mathbf{p}_1\dot{L}_1,\end{aligned} \tag{4.163}$$

that proves that force acting on bead $\mathbf{p}_1L_1$ aligns in direction $\mathbf{p}_1$ as soon as $\mathscr{F}=1$.

The projection of force $\mathbf{F}_1^H$ in the direction $\mathbf{p}_1$ is the one that causes the spring extension, i.e.

$$\begin{aligned}2\mathscr{K}_1(L_1-L_1^0)&=\xi L_1\left((1-\mathscr{F})\mathbf{p}_1^T\cdot\mathbf{D}\cdot\mathbf{p}_1+\mathscr{F}\left(\mathbf{p}_1^T\cdot\mathbf{D}\cdot\mathbf{p}_1\right)\right)-\xi\dot{L}_1=\\ &\xi L_1\mathbf{p}_1^T\cdot\mathbf{D}\cdot\mathbf{p}_1-\xi\dot{L}_1,\end{aligned} \tag{4.164}$$

that is

$$\dot{L}_1=-\mathscr{K}_1^*(L_1-L_1^0)+L_1\mathbf{p}_1^T\cdot\mathbf{D}\cdot\mathbf{p}_1, \tag{4.165}$$

with $\mathscr{K}_1^*=\frac{2\mathscr{K}_1}{\xi}$.

Obviously repeating the rationale for $\mathbf{F}_2^H$ it results that

$$\dot{L}_2=-\mathscr{K}_2^*(L_2-L_2^0)+L_2\mathbf{p}_2^T\cdot\mathbf{D}\cdot\mathbf{p}_2, \tag{4.166}$$

with again $\mathscr{K}_2^*=\frac{2\mathscr{K}_2}{\xi}$.

4.3.6 Dilute polymers solutions

By assuming extensible beads connectors instead of rigid dumbbells, the resulting models describe accurately some viscoelastic features of dilute polymer solutions. In this case, linear macromolecules are crudely represented by two beads connected by an extensible (linear or non-linear) spring.

In that follows we are summarizing some of the most usual microstructural models based on this representation. We then start by considering models based on a

single connector, to finish with the consideration of the more general (and more complex) Multi-Bead-Spring – MBS –.

4.3.6.1 Linear and nonlinear elastic dumbells

We start by considering two beads connected by an elastic spring (Fig. 4.5) of null reference length, i.e. $L_0 = 0$. In fact the spring reference length represent the equilibrium end-to-end distance of a macromolecule idealized as a sequence of beads distributed along its contour and connected by rigid rods. Relative rotation of consecutive rods is allowed at the common bead. In absence of forces the end-to-end averaged distance vanishes justifying the fact of considering a null reference length of the elastic spring. For a complete description the interested reader can refer to [49].

Linear spring

Considering again the system depicted in Fig. 4.5, neglecting Brownian forces, assuming a linear spring with rigidity $\mathscr{K}$ and null reference length, and proceeding in a similar way that in previous section, we obtain model (4.157) with $L_0 = 0$

$$\begin{cases} \dot{\mathbf{p}} = \nabla \mathbf{v} \cdot \mathbf{p} - \nabla \mathbf{v} : (\mathbf{p} \otimes \mathbf{p})\mathbf{p} \\ \dot{L} = -\frac{2\mathscr{K}}{\xi} L + \nabla \mathbf{v} : (\mathbf{p} \otimes \mathbf{p}) L) \end{cases} . \tag{4.167}$$

The time evolution of the connector $\mathbf{q} = \mathbf{p}L$ reads taking into account both expressions in (4.167)

$$\dot{\mathbf{q}} = \dot{\mathbf{p}}L + \mathbf{p}\dot{L} = \nabla \mathbf{v} \cdot \mathbf{q} - \frac{2\mathscr{K}}{\xi}\mathbf{q}, \tag{4.168}$$

in which we identify the affine deformation $\nabla \mathbf{v} \cdot \mathbf{q}$, that now is not constrained by a constant length as it was the case when considering the unit vector $\mathbf{p}$, and the elastic term proportional to the spring stretching $\mathbf{q}$ (remember that the spring reference length is zero).

Now, the mesoscopic model involving the pdf $\Psi(\mathbf{x}, t, \mathbf{q})$ results in the Fokker-Planck equation

$$\frac{\partial \Psi}{\partial t} + \nabla_x \cdot (\mathbf{v}\Psi) + \nabla_q \cdot (\dot{\mathbf{q}}\Psi) = 0, \tag{4.169}$$

where for the moment Brownian effects are neglected. The first two terms in the previous equation can be grouped into the material derivative $\frac{d}{dt}$, and then it allows to rewrite it as

$$\frac{d\Psi}{dt} + \nabla_q \cdot (\dot{\mathbf{q}}\Psi) = 0. \tag{4.170}$$

To define the meso-to-macro bridge we define the conformation tensor $\mathbf{c}(\mathbf{x}, t)$ from

$$\mathbf{c}(\mathbf{x},t) = \int_{\mathbb{R}^3} \mathbf{q} \otimes \mathbf{q} \Psi(\mathbf{x},t,\mathbf{q})\, d\mathbf{q}. \tag{4.171}$$

In order to determine the equation governing its evolution, $\dot{\mathbf{c}}$, we multiply both members of Eq. (4.170) by $\mathbf{q} \otimes \mathbf{q}$ and then we integrate in the configurational space in which $\mathbf{q}$ is defined, $\mathbb{R}^3$, making use of the integration by parts, to obtain

$$\frac{d\mathbf{c}}{dt} = \nabla \mathbf{v} \cdot \mathbf{c} + \mathbf{c} \cdot (\nabla \mathbf{v})^T - \frac{4\mathscr{K}}{\xi}\mathbf{c}. \tag{4.172}$$

To consider Brownian effects we write the equilibrium of forces applying on the two beads, the first located at $\mathbf{r}_1$ and the second at $\mathbf{r}_2$, with the connector $\mathbf{q}$ defined from $\mathbf{q} = \mathbf{r}_2 - \mathbf{r}_1$:

$$-\xi(\dot{\mathbf{r}}_2 - \mathbf{v}_0 - \nabla \mathbf{v} \cdot \mathbf{r}_2) - K_b T \frac{\partial}{\partial \mathbf{r}_2} \ln(\Psi) - \mathbf{F}^C = \mathbf{0}, \tag{4.173}$$

where ξ is the drag coefficient, $\mathbf{v}_0$ is the fluid velocity at the origin of coordinates, K_b is the Boltzmann's constant, T is the absolute temperature and $\mathbf{F}^C$ is the elastic force in the spring. Here, because the assumed linearity, $\mathbf{F}^C$ is proportional to its length and act along the connector (spring) direction, i.e. $\mathbf{F}^C = \mathscr{K}\mathbf{q}$. We consider the random force involving the logarithm of the the distribution function Ψ to recover a diffusion term in the associated Fokker-Planck equation.

The balance of forces at the other bead reads

$$-\xi(\dot{\mathbf{r}}_1 - \mathbf{v}_0 - \nabla \mathbf{v} \cdot \mathbf{r}_1) - K_b T \frac{\partial}{\partial \mathbf{r}_1} \ln(\Psi) + \mathbf{F}^C = \mathbf{0}. \tag{4.174}$$

By subtracting the second one to the first one, taking into account

$$\begin{cases} \frac{\partial}{\partial \mathbf{r}_2} = \frac{\partial}{\partial \mathbf{q}} \frac{\partial \mathbf{q}}{\partial \mathbf{r}_2} = \frac{\partial}{\partial \mathbf{q}} \\ \frac{\partial}{\partial \mathbf{r}_1} = \frac{\partial}{\partial \mathbf{q}} \frac{\partial \mathbf{q}}{\partial \mathbf{r}_1} = -\frac{\partial}{\partial \mathbf{q}} \end{cases}, \tag{4.175}$$

it results that

$$-\xi(\dot{\mathbf{q}} - \nabla \mathbf{v} \cdot \mathbf{q}) - 2K_b T \frac{\partial}{\partial \mathbf{q}} \ln(\Psi) - 2\mathbf{F}^C = \mathbf{0}, \tag{4.176}$$

from which the expression of $\dot{\mathbf{q}}$ can be extracted

$$\dot{\mathbf{q}} = \nabla \mathbf{v} \cdot \mathbf{q} - \frac{2K_b T}{\xi} \frac{\partial}{\partial \mathbf{q}} \ln(\Psi) - \frac{2}{\xi}\mathbf{F}^C, \tag{4.177}$$

and using the linear behavior of the elastic spring

$$\dot{\mathbf{q}} = \nabla \mathbf{v} \cdot \mathbf{q} - \frac{2K_b T}{\xi} \frac{\partial}{\partial \mathbf{q}} \ln(\Psi) - \frac{2\mathscr{K}}{\xi}\mathbf{q}, \tag{4.178}$$

It can be noticed that in absence of Brownian effects and for a linear spring Eq. (4.178) reduces to the one previously obtained, Eq. (4.168).

The mesoscopic model is defined as previously by

$$\frac{\partial \Psi}{\partial t} + \nabla_x \cdot (\mathbf{v}\Psi) + \nabla_q \cdot (\dot{\mathbf{q}}\Psi) = 0, \tag{4.179}$$

that making use of the material derivative material derivative reduces to

$$\frac{d\Psi}{dt} + \nabla_q \cdot (\dot{\mathbf{q}}\Psi) = 0, \tag{4.180}$$

where now $\dot{\mathbf{q}}$ is given by Eq. (4.178) that includes Brownian effects.

In order to determine the equation governing the evolution of the conformation tensor $\dot{\mathbf{c}}$, when Brownian effects are retained in the model, we multiply both members of Eq. (4.180) by $\mathbf{q} \otimes \mathbf{q}$ and then we integrate in the configurational space $\mathbb{R}^3$, making use of the integration by parts, to obtain

$$\frac{d\mathbf{c}}{dt} = \nabla \mathbf{v} \cdot \mathbf{c} + \mathbf{c} \cdot (\nabla \mathbf{v})^T - \frac{4\mathscr{K}}{\xi}\mathbf{c} + \frac{4K_bT}{\xi}\mathbf{I}. \tag{4.181}$$

If the extra-stress is assumed given by the Kramer's expression, with n the number of elastic dumbbells per unit volume, it results

$$\tau + nK_bT\mathbf{I} = n\langle \mathbf{F}^c \otimes \mathbf{q} \rangle = n\mathscr{K}\mathbf{c}, \tag{4.182}$$

where the term $nK_bT\mathbf{I}$ is isotropic and then it does not have any rheological consequence.

By substituting expression (4.182) into Eq. (4.181) it results

$$\frac{1}{n\mathscr{K}}\left(\frac{d\tau}{dt} - \nabla \mathbf{v} \cdot \tau - \tau \cdot (\nabla \mathbf{v})^T\right) + \frac{4}{n\xi}\tau = 2nK_bT\mathbf{D}, \tag{4.183}$$

where the upper-convected derivative $\frac{\delta}{\delta t}$ can be identified, leading to

$$\frac{1}{n\mathscr{K}}\frac{\delta \tau}{\delta t} + \frac{4}{n\xi}\tau = 2nK_bT\mathbf{D}, \tag{4.184}$$

that by introducing the parameters

$$\begin{cases} \lambda = \frac{\xi}{4\mathscr{K}} \\ \eta_p = \frac{n^2 K_b T \xi}{4} \end{cases}, \tag{4.185}$$

leads to the viscoelastic Oldroyd-B model

$$\lambda \frac{\delta \tau}{\delta t} + \tau = 2\eta_p \mathbf{D}. \tag{4.186}$$

Nonlinear

spring

When considering a nonlinear spring behavior, the time evolution of the connector $\mathbf{q}$ reads

$$\dot{\mathbf{q}} = \nabla \mathbf{v} \cdot \mathbf{q} - \frac{2\mathscr{K}(q)}{\xi}\mathbf{q}, \tag{4.187}$$

with $q = \|\mathbf{q}\|$.

Now, the mesoscopic model involving the pdf $\Psi(\mathbf{x},t,\mathbf{q})$ results in the Fokker-Planck equation

$$\frac{\partial \Psi}{\partial t} + \nabla_x \cdot (\mathbf{v}\Psi) + \nabla_q \cdot (\dot{\mathbf{q}}\Psi) = 0, \tag{4.188}$$

or using the material derivative $\frac{d}{dt}$

$$\frac{d\Psi}{dt} + \nabla_q \cdot (\dot{\mathbf{q}}\Psi) = 0. \tag{4.189}$$

The non linear term $\mathscr{K}(q)$ makes impossible, in the general case, to obtain a closed equation for the evolution of the conformation tensor and then for the extra-stress tensor (constitutive equation). The introduction of particular closures makes possible the obtention of closed equations as is the case of FENE-P models (see chapter 1 in [12]).

Thus the microscopic counterpart of the viscoelastic Oldroyd-B model can be derived by using a linear spring, and the so-called FENE (Finitely Extensible Non Linear Elastic) model is obtained by considering the connector force

$$\mathbf{F}^c = \mathscr{K}(q)\mathbf{q} = \frac{1}{1 - \frac{\|\mathbf{q}\|^2}{b}}\mathbf{q}, \tag{4.190}$$

where $\sqrt{b}$ is the maximum stretching of the spring connector.

4.3.6.2 Multi-Bead-Spring models

As depicted in Fig. 4.6, the Multi-Bead-Spring – MBS – chain consists of $N+1$ beads connected by N springs. The bead serves as an interaction point with the solvent and the spring contains the local stiffness information depending on local stretching (see [13, 26] and the references therein for additional details).

The dynamics of the chain is governed by hydrodynamic, Brownian and connector (spring) forces. If we denote by $\dot{\mathbf{r}}_j$ the velocity of the bead j and by $\dot{\mathbf{q}}_j$ the velocity of the spring connector j, then we obtain

$$\dot{\mathbf{q}}_j = \dot{\mathbf{r}}_{j+1} - \dot{\mathbf{r}}_j; \quad j = 1, \cdots, N. \tag{4.191}$$

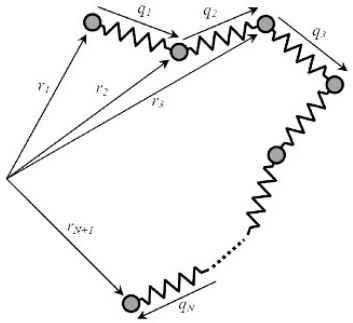

Fig. 4.6 MBS model of a polymer chain

The kinetic theory approach consists in introducing the microstructutal conformation from the pdf $\Psi(\mathbf{x},t,\mathbf{r}_1,\cdots,\mathbf{r}_{N+1})$ or in an equivalent manner, making use of the connector vectors, $\Psi(\mathbf{x},t,\mathbf{q}_1,\cdots,\mathbf{q}_N)$.

The force balance at each bead reads

$$\underbrace{-\xi(\dot{\mathbf{r}}_j-\mathbf{v}_0-\nabla\mathbf{v}\cdot\mathbf{r}_j)}_{\text{Hydrodynamic contribution}}\underbrace{-K_bT\frac{\partial}{\partial\mathbf{r}_j}\ln(\Psi)}_{\text{Brownian contribution}}\underbrace{+\mathbf{F}_j^c-\mathbf{F}_{j-1}^c}_{\text{Connector forces}}=\mathbf{0}, \tag{4.192}$$

where ξ is the drag coefficient, $\mathbf{v}$ is the velocity field, $\mathbf{v}_0$ is the fluid velocity and the origin of coordinates, K_b is the Boltzmann's constant and T is the absolute temperature.

From Eqs. (4.191) and (4.192) it results that:

$$\dot{\mathbf{q}}_j=\nabla\mathbf{v}\cdot\mathbf{q}_j-\frac{1}{\xi}\sum_{k=1}^{N}\mathbf{A}_{jk}\left(K_bT\nabla_{\mathbf{q}_k}\mathbf{ln}(\Psi)+\mathbf{F}_k^c\right) \tag{4.193}$$

where $\nabla_{\mathbf{q}_k}=\frac{\partial}{\partial\mathbf{q}_k}$ and $\mathbf{A}$ is the Rouse's matrix with components

$$\mathbf{A}_{jk}=\begin{cases}2 & \text{if } k=j\\ -1 & \text{if } k=j\pm1\\ 0 & \text{otherwise}\end{cases}. \tag{4.194}$$

In the Rouse model the connector force $\mathbf{F}^c$ is a linear function of the connector vector, but FENE springs previously introduced can be also used.

The pdf involving the physical coordinates (espace and time) and the conformational coordinates (connector vectors) $\Psi(\mathbf{x},t,\mathbf{q}_1,\cdots,\mathbf{q}_N)$ is defined in a space of dimension $3+1+3N$, implying the so-called curse of dimensionality when N increases.

The conservation balance related to the distribution function $\Psi(\mathbf{x},t,\mathbf{q}_1,\cdots,\mathbf{q}_N)$ reads

$$\frac{\partial \Psi}{\partial t} + \nabla_x \cdot (\mathbf{v}\Psi) = -\sum_{j=1}^{N} \nabla_{\mathbf{q}_j} \cdot (\dot{\mathbf{q}}_j \, \Psi). \tag{4.195}$$

By Introducing Eq. (4.193) it results:

$$\begin{aligned} \frac{\partial \Psi}{\partial t} + \nabla_x \cdot (\mathbf{v}\Psi) = -\sum_{j=1}^{N} \nabla_{\mathbf{q}_j} \cdot \left(\left(\nabla \mathbf{v} \cdot \mathbf{q}_j - \frac{1}{\xi} \sum_{k=1}^{N} \mathbf{A}_{jk} \, \mathbf{F}_k^c \right) \Psi \right) + \\ + \frac{K_b T}{\zeta} \sum_{j=1}^{N} \nabla_{\mathbf{q}_j} \cdot \left(\sum_{k=1}^{N} \mathbf{A}_{jk} \nabla_{\mathbf{q}_k} \Psi \right). \end{aligned} \tag{4.196}$$

This kind of model seems particularly suitable for representing molecular chains composed by rigid segments as in the case of the DNA. Other variants can be defined, for example by restricting the free rotation of each two consecutive rods by introducing a rotational spring at each bead. In all these models the expression of the rods rotational velocity (4.193) must be reevaluated depending on the considered physics.

4.3.7 Polymer melts

In most polymer processing operations such as injection molding, film blowing and extrusion, the polymers are in the molten state. A widely applied class of molecular-based models for concentrated polymer solutions and melts relies on the notion of reptation motion.

The key idea of this model is the application of the reptation mechanism introduced by De-Gennes [23] to a tube (along which the molecule can move) in order to describe the viscoelastic behavior of entangled polymers. The molecule is described as sliding or reptating through a tube whose contours are defined by the locus of entanglements with neighboring molecules. The motion of a molecular chain in any other direction that the one defined by the tube axis is strongly restricted, except at both tube ends, where it can move in any possible direction. The tube moves itself due to two mechanisms: (i) by means of the motion of the central chain itself, which partially leaves its original tube, for extending it in other directions, and (ii) by the fluctuation induced by the motions of the neighbor chains defining the tube lateral border.

In addition to the reptation mechanism, the Doi-Edwards model [25] assumes affine tube deformation induced by the macroscopic flow but neglects other phenomena like the stretch of the chain, the Convective Constraint Release -CCR- or the double reptation.

Within the reptation picture and these assumptions, the dynamics of a single tube segment represented by the unit $\mathbf{u}$ (tangent to the tube) is given by the affine deformation

$$\dot{\mathbf{u}} = \nabla \mathbf{v} \cdot \mathbf{u} - (\nabla \mathbf{v} : (\mathbf{u} \otimes \mathbf{u}))\mathbf{u}. \tag{4.197}$$

The molecule defining and occupying the tube at the initial time, is equipped with a contour length coordinate s where $s = 0$ and $s = 1$ represent the chain ends.

The distribution function involved in the Doi & Edwards model depends on the physical space and time and also on the conformation coordinates $\mathbf{u}$ and s, $\Psi(\mathbf{x},t,\mathbf{u},s)$, where $\Psi(\mathbf{x},t,\mathbf{u},s)d\mathbf{u}ds$ represents the joint probability that at position $\mathbf{x}$ and time t, a tube segment having the orientation in the interval $[\mathbf{u},\mathbf{u}+d\mathbf{u}]$ contains the chain segment labelled in the interval $[s,s+ds]$. Thus, the configuration space results $\mathscr{S}\times[0,1]$.

The balance of $\Psi(\mathbf{x},\mathbf{u},s,t)$ results

$$\frac{\partial\Psi}{\partial t}+\nabla_x\cdot(\mathbf{v}\Psi)+\nabla_u\cdot(\dot{\mathbf{u}}\Psi)+\nabla_s(q_s)=0, \tag{4.198}$$

where the reptation flux can be modeled from a diffusion term

$$q_s=-D_r\frac{\partial\Psi}{\partial s}, \tag{4.199}$$

whose diffusion coefficient D_r is related to the reptation characteristic time τ_r for a chain to come out the tube by reptation,

$$D_r=\frac{1}{\pi^2\tau_r}. \tag{4.200}$$

Thus, Eq. (4.198) can be written as:

$$\frac{\partial\Psi}{\partial t}+\nabla_x\cdot(\mathbf{v}\Psi)+\nabla_u\cdot(\dot{\mathbf{u}}\Psi)-D_r\frac{\partial^2\Psi}{\partial s^2}=0. \tag{4.201}$$

To solve the Fokker-Planck equation, one needs to prescribe appropriate boundary conditions at the conformational domain boundaries $s = 0$ and $s = 1$ (the orientation coordinate being defined on the unit sphere does not require enforcing any boundary condition). The usual choice is assuming an isotropic orientation distribution at both ends (even if other choices could be more pertinent in some situations), which reads

$$\Psi(\mathbf{x},t,\mathbf{u},s=0)=\Psi(\mathbf{x},t,\mathbf{u},s=1)=\frac{1}{4\pi}. \tag{4.202}$$

Knowing the distribution function, the stress can be computed from

$$\tau(\mathbf{x},t)=G\int_{\mathscr{S}\times[0,1]}\mathbf{u}\otimes\mathbf{u}\;\Psi(\mathbf{x},t,\mathbf{u},s)\;d\mathbf{u}ds, \tag{4.203}$$

where G is an elastic modulus.

However, the Doi-Edwards model seems to be too simplistic to take into account some features observed experimentally. More advanced kinetic theory models were proposed including chain stretching, double reptation and convective constraint release.

4.3.8 Liquid Crystalline Polymers

Important difficulties persist in the numerical calculation of flows of complex fluids consisting of highly anisotropic particles. Most of these difficulties stem from the necessity to capture the rich dynamic fluid behavior, which spans both isotropic and anisotropic fluid microstructures (nematic, chiral nematic, smectic etc). For example, models describing single particle orientation in a dilute suspension, i.e. in the absence of inter-particle interaction, as the one deeply described previously based on the Jeffery's model, are not able to describe the behavior of a nematic suspension.

The successful treatment of collective flow-orientation phenomena appearing at high concentrations requires the consideration of interparticle interaction, either explicitly like in microscopic liquid-cristal models – LC – or in a mean-field sense. There are notable examples of mean field approaches to anisotropic particle interaction described within the kinetic theory framework.

Different closure approximations have been proposed for alleviating the numerical simulation of LC models by proceeding at the macroscopic scale. The impact of these approximations on the rheological response can be significant, even if some of them retain the main features of the kinetic theory model.

An appealing choice that allows circumventing the introduction of such approximations consists in solving directly the Fokker-Planck equation related to the kinetic theory description of LC models. In this section we consider the Fokker-Planck equation associated with Doi's model.

In order to describe the fluid microstructure we firstly define the unit vector $\mathbf{u}$ describing the orientation of the liquid crystal (LC) molecule axis. Now, the distribution function which gives the probability of finding, at a certain point $\mathbf{x}$ and time t, molecules aligned in the direction $\mathbf{u}$ is represented by $\Psi(\mathbf{x},\mathbf{u},t)$, defined by: $\Psi(\mathbf{x},\mathbf{u},t) : \mathbb{R}^3 \times \mathscr{S} \times \mathbb{R}^+ \to \mathbb{R}^+$. The dynamics of the evolution of this distribution function is induced by (i) hydrodynamic effects, (ii) Brownian effects and (iii) LC-molecules interaction described by a nematic potential. The corresponding Fokker-Planck equation related to Doi's model writes

$$\frac{\partial \Psi}{\partial t} + \nabla_x \cdot (\mathbf{v}\Psi) =$$

$$-\nabla_u \cdot (\dot{\mathbf{u}}\,\Psi) + \nabla_u \cdot (D_r \nabla_u \Psi) + \nabla_u \cdot \left(D_r \Psi \nabla_u \left(\frac{V(\mathbf{u})}{K_b T} \right) \right), \tag{4.204}$$

where the last two terms describe diffusion and nematic effects, K_b is Boltzmann's constant, D_r the diffusion coefficient describing the Brownian effects, T the absolute temperature and $\mathbf{v}$ the fluid velocity field. The rotary velocity dictated by an affine deformation assumption

$$\dot{\mathbf{u}} = \nabla \mathbf{v} \cdot \mathbf{u} - (\nabla \mathbf{v} : (\mathbf{u} \otimes \mathbf{u}))\,\mathbf{u}. \tag{4.205}$$

We can notice that removing the last term in Eq. (4.204) involving the nematic potential $V(\mathbf{u})$ reduces to the kinetic theory description of rods suspensions previously described.

A frequently used form for the nematic potential is

$$V(\mathbf{u}) = -\frac{3}{2} U K_b T (\mathbf{u} \otimes \mathbf{u}) : \mathbf{S}, \tag{4.206}$$

where U is a dimensionless interaction potential and the second order traceless orientation tensor $\mathbf{S}$ is defined by

$$\mathbf{S} = \langle \mathbf{u} \otimes \mathbf{u} \rangle - \frac{\mathbf{I}}{3}, \tag{4.207}$$

with the averaging $\langle \bullet \rangle$ defined on the unit sphere $\mathscr{S}$ by the second moment of the orientation distribution (as was the case when considering rigid rods)

$$\langle \mathbf{u} \otimes \mathbf{u} \rangle = \int_{\mathscr{S}} \mathbf{u} \otimes \mathbf{u} \; \Psi(\mathbf{x}, \mathbf{u}, t) \; d\mathbf{u}. \tag{4.208}$$

To illustrate the physical meaning of the nematic potential we are considering a 2D molecular orientation distribution (in absence of macroscopic flow) where most molecules are fully aligned in a certain direction, for example in the x-direction. In this case the different entities appearing in the nematic potential result

$$\langle \mathbf{u} \otimes \mathbf{u} \rangle = \left\langle \begin{pmatrix} \cos^2\varphi & \cos\varphi \sin\varphi \\ \cos\varphi \sin\varphi & \sin^2\varphi \end{pmatrix} \right\rangle \approx \begin{pmatrix} 1 & 0 \\ 0 & 0 \end{pmatrix}, \tag{4.209}$$

that implies

$$\mathbf{S} = \langle \mathbf{u} \otimes \mathbf{u} \rangle - \frac{\mathbf{I}}{2} \approx \begin{pmatrix} \frac{1}{2} & 0 \\ 0 & -\frac{1}{2} \end{pmatrix}, \tag{4.210}$$

and then

$$V(\mathbf{u}) = -\frac{3}{2} U K_b T (\mathbf{u} \otimes \mathbf{u}) : \mathbf{S} = -\beta \left(\frac{\cos^2(\varphi)}{2} - \frac{\sin^2(\varphi)}{2} \right), \tag{4.211}$$

where $\beta = \frac{3}{2} U K_b T$. Now, we evaluate $\nabla_u V(\mathbf{u})$

$$\nabla_u V(\mathbf{u}) = \frac{\partial V(\varphi)}{\partial \varphi} = 2\beta \cos\varphi \sin\varphi, \tag{4.212}$$

that allows to define the nematic pseudo-rotary velocity

$$\dot{\varphi}_{nem} = -3 U D_r \cos(\varphi) \sin(\varphi), \tag{4.213}$$

such that Eq. (4.204) in absence of flow reduces to

$$\frac{\partial \Psi}{\partial t} = D_r \frac{\partial^2 \Psi}{\partial \varphi^2} - \frac{\partial}{\partial \varphi}(\dot{\varphi}_{nem}\, \Psi), \tag{4.214}$$

from which we can conclude that Brownian effects induce a tendency towards a random distribution whereas the nematic term tends to concentrate more and more the orientation distribution on the direction along which most of the molecules are oriented, in the present case $\varphi = 0$. This tendency can be noticed by simple inspection of Eq. (4.213): there are two equilibrium positions (where the "nematic" velocity vanishes) at $\varphi = 0$ and $\varphi = \frac{\pi}{2}$. However that velocity in $\varphi = 0 \pm \varepsilon$ tends to approach the molecule to $\varphi = 0$, whereas in $\varphi = \frac{\pi}{2} \pm \varepsilon$ the velocity moves apart the molecule that approach the other equilibrium position $\varphi = 0$, proving that $\varphi = 0$ is the single stable orientation.

4.3.9 Carbon-Nanotubes suspensions: introducing aggregation effects

Carbon nanotubes (CNTs) belong to a relatively new class of fibrous material, with a length scale between that of polymer chain and classical synthetic fibers. Because of their high mechanical strength, low density, high thermal and electrical conductivity, they can potentially be used for high-performance nanocomposites or nanodevices. Since most applications involve suspending CNTs in a matrix, it is important to understand and model the rheology of CNT suspensions. The rheology of CNTs suspended in different matrices has been studied experimentally by a number of researchers. A significant shear-thinning characteristic for untreated CNTs suspended within an epoxy resin was reported and CNT aggregates were optically observed.

Although different empirical models such as the Cross model, the Carreau model and the Krieger-Dougherty model can be used to describe the evolution of flow curves for CNT suspensions, knowing the microstructure of CNT suspensions is of equal importance as it is intimately related to the final physical properties of CNT composite materials.

In the context of short-fiber suspensions modeling (previously addressed), a simple orientation model could be used to describe the evolution of steady shear viscosity by coupling the flow kinematics with the fiber orientation. In the first modeling attempt, it was assumed that CNTs can essentially be modeled as short rigid fibers which can rotate and align in a shear flow and that the evolution of the viscosity contribution due to the presence of CNTs depends only on the orientation of CNTs.

In the simple orientation mesoscopic model making use of the Fokker-Planck equation and the constitutive law previously introduced N_p and D_r were the key adjustable parameters to fit to the experimental data. The model was found to be successful in capturing the shear thinning characteristic for some surface-treated CNT suspensions where no optically resolvable CNT aggregate was observed [40].

However, that model with the use of a single D_r and N_p values, failed to fit the experimental flow curves for untreated CNT suspensions, where the extent of viscosity enhancement was very pronounced at low shear rates. It is clear that a simple orientation explanation was not sufficient to describe the observed viscosity enhancement and it is believed that the extra contribution to shear viscosity at low shear rates is due to the presence of CNT aggregates, which were experimentally observed in optical microstructure studies.

The simple orientation model could not describe the shear-thinning characteristic for untreated CNT suspensions, and therefore a new model called the Aggregation/Orientation – AO – model was developed. The model essentially considered a hierarchy of CNT aggregate structures in an untreated CNT suspension, where the shear viscosity was controlled not only by CNT orientation, but also by the aggregation state of CNTs in the suspension. The Fokker-Planck description was modified to incorporate aggregation/disaggregation kinetics and a detailed derivation for the AO model is included in this section.

The aggregation/orientation distribution function in the AO model is written as $\Psi(\mathbf{x},\mathbf{p},n,t) : \mathbb{R}^3 \times \mathscr{S} \times [0,1] \times \mathbb{R}^+ \to \mathbb{R}^+$, where $n \in [0,1]$ describes the state of aggregation: $n = 0$ corresponds to CNTs that are free from entanglement and $n = 1$ represents a CNT aggregate network. For a steady and homogeneous flow, the aggregation/orientation distribution reduces to $\Psi(\mathbf{p},n)$, which describes the fraction of CNTs orientated in the direction $\mathbf{p}$ and belonging to a population n. $\Psi(\mathbf{p},n)$ now contains information about both CNT orientation and the aggregation state and the remaining task is to modify the Fokker-Planck equation accordingly.

For an arbitrary population n (where $n \neq 0$ and $n \neq 1$), the population can increase as a result of the aggregation of smaller aggregates ($r < n$) or the disaggregation of larger aggregates ($r > n$). On the other hand, the population n can also decreases because of the disaggregation of population n originating less entangled aggregates ($r < n$) or the aggregation forming more entangled aggregates ($r > n$). If a constant aggregation velocity (v_c) and a constant disaggregation velocity (v_d) are assumed, the following balance can be written for the population n

$$\begin{aligned} \dot{\mathscr{A}}(n) = v_c \int_0^n \Psi(\mathbf{p},r)\Psi(\mathbf{p},n-r)\, dr + v_d \int_n^1 \tfrac{1}{r}\Psi(\mathbf{p},r)\, dr - \\ v_d \Psi(\mathbf{p},n) - v_c \Psi(\mathbf{p},n) \int_0^{1-n} \Psi(\mathbf{p},r)\, dr, \end{aligned} \tag{4.215}$$

where it has been assumed that the desagregation of population $r > n$ produces a uniform distribution of smaller aggregates, justifying the factor $1/r$ in the second integral term.

The resulting Fokker-Planck equation reads

$$\frac{\partial \Psi}{\partial t} + \nabla_x \cdot (\mathbf{v}\Psi) = -\nabla_p \cdot (\dot{\mathbf{p}}\,\Psi) + \nabla_p \cdot (D_r \nabla_{\mathbf{p}} \Psi) + \dot{\mathscr{A}}(n), \tag{4.216}$$

with the rotary velocity given again by Jeffery's equation for rods (infinite aspect ratio ellipsoids)

$$\dot{\mathbf{p}} = \nabla \mathbf{v} \cdot \mathbf{p} - (\nabla \mathbf{v} : (\mathbf{p} \otimes \mathbf{p}))\,\mathbf{p}. \tag{4.217}$$

The solution of this model allowed in [39] to recover the main rheological features of untreated CNT suspensions.

4.3.10 Microstructural description of flowing foams

Aqueous foams are concentrated dispersions of gas bubbles in a surfactant solution. Their structures are organized over a large range of length scales.

The proposal of macroscopic constitutive equations is a key point to address the modeling and simulation of industrial processes involving the flow of foams. However, in general these constitutive equations remain too phenomenological and even if they allow to predict accurately the flow kinematics, microstructure information remains unaccessible. On the opposite side, fully microscopic simulation allows very detailed descriptions of the foam microstructural evolution, however such approaches fail for addressing scenarios of industrial interest that usually involve the flow in very large and complex 3D geometries.

The most appealing route consists on a macroscopic description making use of appropriate microscropic descriptors. The macroscopic flow model is expected to depend on the cellular structure: cells size, shape and orientation as well as on the fluid rheology and the surface tension. Moreover, cell shape and orientation changes are induced by the flow.

The simplest description of a 2D cell, consists of an ellipse ranging from the circular shape to the infinite aspect ratio ellipse (rod). Such an ellipse could be represented from two orthogonal extensible springs, with reference length $2L_0$ and rigidity $\mathscr{K}$. In a previous section the kinematics of linear elastic dumbbells was carried out, and now it becomes the starting point for elaborating the cell conformation.

Incompressible cells

If we assume an ellipse (bubble) with constant volume, we must ensure that $\frac{d(L_1 L_2)}{dt} = 0$, i.e. $\dot{L}_1 L_2 + L_1 \dot{L}_2 = 0$ that using Eqs. (4.165) and (4.166) results

$$\dot{L}_1 L_2 + L_1 \dot{L}_2 = -\mathscr{K}_1^*(L_1 - L_1^0)L_2 - \mathscr{K}_2^*(L_2 - L_2^0)L_1 +$$

$$L_1 L_2 \mathbf{D} : (\mathbf{p}_1 \otimes \mathbf{p}_1 + \mathbf{p}_2 \otimes \mathbf{p}_2)\,. \tag{4.218}$$

Taking into account $(\mathbf{p}_1 \otimes \mathbf{p}_1 + \mathbf{p}_2 \otimes \mathbf{p}_2) = \mathbf{I}$ and the flow incompressibility $\mathbf{D} : \mathbf{I} = 0$, it reduces to

$$\dot{L}_1 L_2 + L_1 \dot{L}_2 = -\mathscr{K}_1^*(L_1 - L_1^0)L_2 - \mathscr{K}_2^*(L_2 - L_2^0)L_1 = 0. \tag{4.219}$$

Now the cell volume conservation implies $L_1 L_2 = L_1^0 L_2^0 = \mathscr{V}$ that leads to

$$\mathscr{V}(\mathscr{K}_1^* + \mathscr{K}_2^*) = \mathscr{K}_1^* L_1^0 L_2 + \mathscr{K}_2^* L_2^0 L_1 \tag{4.220}$$

In order to close the model we assume that, in addition of the elastic spring accounting for the surface tension effects, an extra force F^I must exist in order to ensure the volume conservation.

Thus, following the rationale introduced in section 4.3.5.1, equilibrium at beads $\mathbf{p}_1 L_1$ and $\mathbf{p}_2 L_2$ read now

$$2\mathscr{K}_1(L_1 - L_1^0) + F^I = \xi L_1 \mathbf{p}_1^T \cdot \mathbf{D} \cdot \mathbf{p}_1 - \xi \dot{L}_1, \tag{4.221}$$

and

$$2\mathscr{K}_2(L_2 - L_2^0) + F^I = \xi L_2 \mathbf{p}_2^T \cdot \mathbf{D} \cdot \mathbf{p}_2 - \xi \dot{L}_2, \tag{4.222}$$

respectively, from which it results that

$$\dot{L}_1 = -\mathscr{K}_1^*(L_1 - L_1^0) + L_1 \mathbf{p}_1^T \cdot \mathbf{D} \cdot \mathbf{p}_1 - F^I, \tag{4.223}$$

and

$$\dot{L}_2 = -\mathscr{K}_2^*(L_2 - L_2^0) + L_2 \mathbf{p}_2^T \cdot \mathbf{D} \cdot \mathbf{p}_2 - F^I. \tag{4.224}$$

The incompressibility then reads

$$\dot{L}_1 L_2 + L_1 \dot{L}_2 = -\mathscr{K}_1^*(L_1 - L_1^0)L_2 - \mathscr{K}_2^*(L_2 - L_2^0)L_1 - F^I(L_1 + L_2) = 0, \tag{4.225}$$

that allows to derive the incompressibility Lagrange multiplier F^I

$$F^I = -\frac{1}{L_1 + L_2}\left(\mathscr{K}_1^*(L_1 - L_1^0)L_2 + \mathscr{K}_2^*(L_2 - L_2^0)L_1\right). \tag{4.226}$$

Thus, finally the kinematic model for the orthogonal elastic bi-dumbell reads:

$$\begin{cases} \dot{\mathbf{p}}_1 = \Omega \cdot \mathbf{p}_1 + \frac{L_1^2 - L_2^2}{L_1^2 + L_2^2}\mathbf{D} \cdot \mathbf{p}_1 - \frac{L_1^2 - L_2^2}{L_1^2 + L_2^2}\left(\mathbf{p}_1^T \cdot \mathbf{D} \cdot \mathbf{p}_1\right)\mathbf{p}_1 \\ \dot{L}_1 = -\mathscr{K}_1^*(L_1 - L_1^0) - F^I + L_1 \mathbf{p}_1^T \cdot \mathbf{D} \cdot \mathbf{p}_1 \\ \dot{L}_2 = -\frac{L_2}{L_1}\dot{L}_1 \\ F^I = -\frac{1}{L_1 + L_2}\left(\mathscr{K}_1^*(L_1 - L_1^0)L_2 + \mathscr{K}_2^*(L_2 - L_2^0)L_1\right) \end{cases}. \tag{4.227}$$

4.3.10.1 Conformation descriptor

The simplest choice for the conformation tensor consists of the second order symmetric tensor $\mathbf{c}$ defined from

$$\mathbf{c} = \frac{L_1^2}{2}(\mathbf{p}_1 \otimes \mathbf{p}_1) + \frac{L_2^2}{2}(\mathbf{p}_2 \otimes \mathbf{p}_2), \tag{4.228}$$

to be introduced into the macroscopic foam flow constitutive equation

$$\sigma = -p\mathbf{I} + \tau = -p\mathbf{I} + 2\eta\mathbf{D} + \mu\mathbf{c}, \tag{4.229}$$

where p is the pressure, that can be viewed as the Lagrange multiplayer associated with the macroscopic flow incompressibility constraint, η the effective homogenized fluid viscosity, and μ the rheological parameter affecting the contribution of the microscopic conformation.

4.3.11 Kinetic theory approach of micro-structural theory of passive mixing

Many chemical engineering processes benefit of good bulk mixing. In such processes, the determination of mixing rate is important in terms of understanding and prediction of mixing time. The understanding allows to define new flows and the associated processes maximizing the mixing rate, but one could also try to optimize other parameters related to the microstructure describing the morphology, characteristic length, shape and orientation

A possible way of quantifying the mixing rate can be derived from the consideration of only one of the basic mechanisms of mixing processes: the increase of the material interface due to the fluid mechanics in absence of interfacial tension and molecular diffusion. The molecular diffusion leads to smooth concentration gradients across the interface. However this mechanism only becomes significant when the interface has increased significantly. It is therefore expected that the overall mixing rate will be closely linked to the rate of mechanical stretching of the interfacial area.

The approaches quantifying the mixing from the increase of the material interface have two important drawbacks: (i) the first one is associated with the difficulty of introducing other additional physics as the one related to the surface tension, and (ii) sometimes the microstructure description needs other information (morphology, characteristic length, shape and orientation, etc.) that the area of the interface evolution cannot provide.

In passive mixing, interfacial energy is negligible and the two phases have identical viscosities. Moreover, the global velocity field can be found independently of the microstructure and then used to evolve the mixture structure, described with some area tensor, very rich from the morphological and microstructural points of view.

In this section we summarize the kinetic theory approach proposed in our former work [18] based on the use of the area tensor considered [52].

4.3.11.1 Morphology description of microstructured fluids

Let's Ω be the domain in which the flow problem is defined. Points in Ω will be referred by $\mathbf{x}$ which is a vector in 2D or 3D. In order to quantify the morphology at any point $\mathbf{x} \in \Omega$ a microscopic representative volume $V(\mathbf{x})$ is considered centered at

that point. This volume results small with respect to the macroscopic scale (related to the variation of the velocity field in Ω) but large enough with respect to the characteristic size of the microstructure. Let's $S(\mathbf{x})$ be the interface within $V(\mathbf{x})$. The second order area tensor $\mathbf{A}$ is then defined as:

$$\mathbf{A}(\mathbf{x}) = \frac{1}{V(\mathbf{x})} \int_{S(x)} \mathbf{n} \otimes \mathbf{n} \, dS, \tag{4.230}$$

where $\mathbf{n}$ represents the unit vector defined on the interface $S(\mathbf{x})$ assuming that it is pointing towards the continuous phase (the discrete one is the one with lower volume fraction). This area tensor is symmetric and has different appealing properties:

- The first property concerns its trace that we symbolize by $\mathrm{Tr}(\mathbf{A}(\mathbf{x}))$ that taking into account the normality of $\mathbf{n}$ results in

$$\mathrm{Tr}(\mathbf{A}(\mathbf{x})) = \frac{1}{V(\mathbf{x})} \int_{S(\mathbf{x})} (\mathbf{n}_1^2 + \mathbf{n}_2^2 + \mathbf{n}_3^2) \, dS = \frac{1}{V(\mathbf{x})} \int_{S(\mathbf{x})} dS = \frac{\mathbf{S}(\mathbf{x})}{\mathbf{V}(\mathbf{x})} = S_v(\mathbf{x}), \tag{4.231}$$

  where $S_v(\mathbf{x})$ represents the specific surface related to point $\mathbf{x}$, and whose maximization is usually searched in mixing processes.
- If we define the volume fraction of the disperse phase as ϕ then we can define a characteristic length of the microstructure at point $\mathbf{x}$ from the volume of the discrete phase $V_d(\mathbf{x}) = \phi V(\mathbf{x})$:

$$L(\mathbf{x}) \equiv \frac{V_d(\mathbf{x})}{S(\mathbf{x})} = \frac{\phi V(\mathbf{x})}{S(\mathbf{x})} = \frac{\phi}{S_v(\mathbf{x})} = \frac{\phi}{\mathrm{Tr}(\mathbf{A}(\mathbf{x}))}. \tag{4.232}$$

- The microstructure shape and orientation can be easily deduced from the normalized area tensor $\tilde{\mathbf{A}}(\mathbf{x})$ defined as

$$\tilde{\mathbf{A}}(\mathbf{x}) = \frac{\mathbf{A}(\mathbf{x})}{\mathrm{Tr}(\mathbf{A}(\mathbf{x}))}, \tag{4.233}$$

  and represented from an ellipsoid. The eigenvalues of $\tilde{\mathbf{A}}$ allow to compute the length of the ellipsoid axes, since their orientation are given by the associated eigenvectors.

The interest of computing the area tensor, from a given initial condition, at each point of the flow domain and at each time has been justified. However, its evaluation needs the establishment of the partial differential equation governing its evolution. In what follows we are establishing this evolution equation and the closure issue that its solution implies.

To derive the evolution equation of $\mathbf{A}(\mathbf{x})$ we consider the time derivative of vector $\mathbf{n}$ and the surface element dS (standard results in continuum mechanics)

$$\frac{d\mathbf{n}}{dt} = \dot{\mathbf{n}} = -(\nabla \mathbf{v})^{\mathrm{T}} \mathbf{n} + (\nabla \mathbf{v} : (\mathbf{n} \otimes \mathbf{n})) \, \mathbf{n}, \tag{4.234}$$

and

$$\frac{dS}{dt} = -(\nabla \mathbf{v} : (\mathbf{n} \otimes \mathbf{n}))\, dS. \tag{4.235}$$

Introducing Eqs. (4.234) and (4.235) into the time derivative of Eq. (4.230) it results:

$$\frac{d\mathbf{A}}{dt} = -(\nabla \mathbf{v})^{\mathbf{T}} \cdot \mathbf{A} \; - \; \mathbf{A} \cdot \nabla \mathbf{v} + \nabla \mathbf{v} : \mathscr{A}, \tag{4.236}$$

where the dependence of $\mathbf{A}(\mathbf{x})$ on $\mathbf{x}$ has been omitted for the sake of clarity, and where $\mathscr{A}$ denotes the fourth order area tensor defined by:

$$\mathscr{A}(\mathbf{x}) = \frac{1}{V(\mathbf{x})} \int\limits_{S(\mathbf{x})} \mathbf{n} \otimes \mathbf{n} \otimes \mathbf{n} \otimes \mathbf{n}\, dS. \tag{4.237}$$

The main difficulty in solving Eq. (4.236) is precisely related to that fourth order area tensor, as was the case in suspensions composed of rods. Thus, a closure relation expressing that tensor as a function of the second order area tensor is needed. In absence of a general exact closure relation, any closure proposal must be checked carefully because its impact on the computed solution is *a priori* unpredictable.

The formalism associated with the evolution of the area tensor has other advantages. One of them is the simplicity of incorporating other physical effects as for example the surface tension. One could expect that in absence of strain rate the disperse microstructure evolves towards an isotropic state composed of coalescent microspheres, minimizing the specific area. Thus, Doi and Ohta [27] proposed introducing in Eq. (4.236) a source term accounting for such effects

$$\frac{d\mathbf{A}}{dt} = -(\nabla \mathbf{v})^{\mathbf{T}} \cdot \mathbf{A} \; - \; \mathbf{A} \cdot \nabla \mathbf{v} + \nabla \mathbf{v} : \mathscr{A} - a \frac{\sigma}{\eta} S_v^2 \left(\left(\tilde{\mathbf{A}} - \frac{\mathbf{I}}{3} \right) + b \frac{\mathbf{I}}{3} \right), \tag{4.238}$$

where a and b are two material parameters, σ is the surface tension, η the fluid viscosity (we are assuming that both fluids have the same viscosity) and $\mathbf{I}$ the unit tensor. Thus, in absence of strain rate, Eq. (4.238) reduces to:

$$\frac{d\mathbf{A}}{dt} = -a \frac{\sigma}{\eta} S_v^2 \left(\left(\tilde{\mathbf{A}} - \frac{\mathbf{I}}{3} \right) + b \frac{\mathbf{I}}{3} \right), \tag{4.239}$$

proving that the microstructure evolves towards an isotropic state induced by the presence of the term $\tilde{\mathbf{A}} - \frac{\mathbf{I}}{3}$ in which the interface area reduces due to the presence of $-\frac{ab\sigma}{\eta} S_v^2 \frac{\mathbf{I}}{3}$. Even if this model predicts a null long-time specific area, fact that motivated different corrections, we will consider the Doi-Ohta model in the kinetic theory approach that follows.

4.3.11.2 Kinetic theory description of passive mixing

We define the area distribution function $\Psi(\mathbf{x}, \mathbf{n}, t) : \mathbb{R}^3 \times \mathscr{S} \times \mathbb{R}^+ \to \mathbb{R}^+$, given at each point in the physical domain $\mathbf{x} \in \Omega$ and for any time t, the specific surface

$S_v(\mathbf{x})$ orientated in the direction $\mathbf{n}$. Thus, the area tensor can be defined from this area distribution function according to

$$\mathbf{A}(\mathbf{x},t) = \int_{\mathscr{S}} \mathbf{n}\otimes\mathbf{n}\, \Psi(\mathbf{x},\mathbf{n},t)\, d\mathbf{n}. \tag{4.240}$$

The trace of the previous equation reads as expected

$$\mathrm{Tr}(\mathbf{A}(\mathbf{x},t)) = S_v(\mathbf{x},t) = \int_{\mathscr{S}} \mathrm{Tr}(\mathbf{n}\otimes\mathbf{n})\, \Psi(\mathbf{x},\mathbf{n},t)\, d\mathbf{n} = \int_{\mathscr{S}} \Psi(\mathbf{x},\mathbf{n},t)\, d\mathbf{n}. \tag{4.241}$$

The expression of the time derivative of the distribution function reads

$$\frac{\partial \Psi}{\partial t} + \nabla_x \cdot (\mathbf{v}\Psi) = -\nabla_n \cdot (\dot{\mathbf{n}}\Psi) - (\nabla\mathbf{v} : (\mathbf{n}\otimes\mathbf{n}))\, \Psi. \tag{4.242}$$

Eq. (4.242) is close to the Fokker-Planck equation usually employed to describe the microstructure in the rods suspensions considered in the previous sections. However in the present case, because this function is not subjected to a normality condition (Ψ is not a probability density function) there is an additional term (last term in the right member of Eq. (4.242)) taking into account the interface area growing induced by its stretching.

If Eq. (4.242) is solved instead of solving Eq. (4.236) (the latter requires the choice of a closure relation for the fourth order orientation tensor), the area tensor can be computed from Eq. (4.240) without the necessity of introducing any closure relation.

Finally, other physical effects, and in particular the one related to the surface tension, can be easily introduced in the kinetic theory formalism. As before, we are considering the expression of the time derivative of the area tensor (that in the kinetic theory framework is given by Eq. (4.240)), looking for the time derivative of the distribution function Ψ leading to the expression (4.238).

It is easy to prove that the associated kinetic model is given by:

$$\frac{d\Psi}{dt} = -\frac{\partial}{\partial \mathbf{n}}(\dot{n}\, \Psi) - \Big(\nabla\mathbf{v} : (\mathbf{n}\otimes\mathbf{n})\Big)\Psi + \frac{\partial}{\partial \mathbf{n}}\left(\mathscr{D}\frac{\partial \Psi}{\partial \mathbf{n}}\right) + \mathscr{F}, \tag{4.243}$$

where the diffusion coefficient and the source terms result in 2D

$$\mathscr{D} = \frac{a}{4}\frac{\sigma}{\eta} S_v = \frac{a}{4}\frac{\sigma}{\eta}\left(\int_{\mathscr{S}} \Psi(\mathbf{n})\, d\mathbf{n}\right), \tag{4.244}$$

and

$$\mathscr{F} = \frac{a}{4\pi}\frac{\sigma}{\eta}(S_v)^2 b = -\frac{ab}{4\pi}\frac{\sigma}{\eta}\left(\int_{\mathscr{S}} \Psi(\mathbf{n})\, d\mathbf{n}\right)^2. \tag{4.245}$$

4.4 The Chemical Master Equation

Simulating, for example, the behavior of gene regulatory networks is a formidable task for several reasons. At this level of description, only a few molecules (maybe dozens or hundreds) of each species involved in the regulation process are present, and this fact limits the possibility of considering the process as deterministic, as is done very often in most chemical applications. Here, the concept of concentration of the species does not make sense. On the contrary, under some weak hypotheses the system can be considered as Markovian (memory-less), and can be consequently modeled by the so-called Chemical Master Equation – CME–, which is in fact nothing else than a set of ordinary differential equations stating the conservation of the probability distribution function – pdf – P in time.

We consider n different chemical species $\mathscr{S}_i$, $i = 1,\ldots,n$, each one having $K_i + 1$ possible number of individuals $\#s_i \in (0,1,\ldots,K_i)$, $i = 1,\ldots,n$, and a set of m reactions R_j, $j = 1,\ldots,m$ with propensity a_j encoding the reaction rate, expressed from

$$\chi^-_{j,1}s^-_1\mathscr{S}_1 + \ldots + \chi^-_{j,n}s^-_n\mathscr{S}_n \xrightarrow{a_j} \chi^+_{j,1}s^+_1\mathscr{S}_1 + \ldots + \chi^+_{j,n}s^+_n\mathscr{S}_n; \quad j = 1,\cdots,m, \tag{4.246}$$

with $\chi_{j,i}$ controlling the appearance of specie S_i in reaction j. For that purpose χ is a boolean variable taking values 0 or 1.

The system state is defined from $z = (\#s_1,\ldots,\#s_n)$. Thus, reaction j transforms the state $\hat{z} = (\#s^-_1,\ldots,\#s^-_n)$ into z, with $z = \hat{z} + v_j$, where $v_j = (\#s^+_1 - \#s^-_1,\ldots,\#s^+_n - \#s^-_n)$ contains the j-reaction stoichiometry.

As a memoryless random walk, each action corresponds to a Markov equation, the so-called Chemical Master Equation – CME – which tracks the net change in the probability $P(z,t)$

$$\frac{dP(z,t)}{dt} = \sum_{j=1}^{m} a_j(z - v_j,t)P(z - v_j,t) - a_j(z,t)P(z,t), \tag{4.247}$$

with the propensity a_j depending on the system state and time.

Equation 4.247 constitutes a system of linear differential equations that can be integrated from a given initial condition. What is challenging is that it is defined in a space with as many dimensions as the number of different species involved in the regulatory network. If we consider N different species, present at a number n of copies, the number of different possible states of the system is n^N. This number can take the astronomical value of 10^{6000} if we consider some types of proteins, for instance.

To overcome this difficulty, most researches employ Monte Carlo-like algorithms (stochastic simulations). However, Monte Carlo techniques need as many as possible individual realizations of the problem, leading to excessive time consuming simulations, together with great variance in the results. In [7] authors consider the proper generalized decomposition for alleviating the curse of dimensionality. Then, in [8] empirical closures were derived and used within a moment-based description.

4.4.1 Moments-based descriptions

The issue related to the curse of dimensionality, as in many other disciplines as previously described (e.g. suspensions), motivated the replacement of the pdf by some of its moments, since they very often suffice for having a view rich enough on the dynamics of the systems. The use of moment-based descriptions was of major interest in different areas of statistical mechanics and it is more and more considered as an alternative to the discretization of the CME.

A moment represents the expected value of a random variable, z, raised to a certain power. An "expectation" is a specifically defined function in statistics, $E[f(z)] = \int f(z)P(z)dz$ when in continuous spaces or $\sum f(z)P(z)$ in discrete spaces. In general, we can talk about the ith moment as

$$\mu_i(t) = E\left[z^i\right] = \sum_{z=0}^{\infty} P(z,t)z^i. \tag{4.248}$$

A probability distribution is uniquely defined by its full set of moments. Having access to these moments could eliminate the need to solve for the full distribution, depending on what information would be considered important. A special function, called the Moment Generating Function $M(\theta,t)$, is specifically intended for this purpose

$$M(\theta,t) = \sum_{z=0}^{\infty} e^{\theta z}P(z,t). \tag{4.249}$$

By taking the Taylor expansion of $e^{\theta z} = 1 + \frac{(\theta z)^1}{1!} + \frac{(\theta z)^2}{2!} + \frac{(\theta z)^3}{3!} + \cdots$, we can see the moments emerging from this function, the i-th moment associated with the i-th power of θ

$$M(\theta,t) = \mu_0(t) + \frac{\mu_1(t)\theta}{1!} + \frac{\mu_2(t)\theta^2}{2!} + \cdots = \sum_{z=0}^{\infty} \frac{\mu_z(t)\theta^z}{z!}. \tag{4.250}$$

The following equations will be used extensively in the following derivation, so it will be useful to define them before

$$\begin{cases} M(\theta,t) = \sum\limits_{z=0}^{\infty} e^{\theta z}P(z,t) = \sum\limits_{z=0}^{\infty} \frac{\mu_z(t)\theta^z}{z!} \\ \frac{\partial M(\theta,t)}{\partial t} = \sum\limits_{z=0}^{\infty} e^{\theta z}\frac{\partial P(z,t)}{\partial t} \\ \frac{\partial^i M(\theta,t)}{\partial \theta^i} = \sum\limits_{z=0}^{\infty} e^{\theta z}P(z,t)z^i = \sum\limits_{z=0}^{\infty} \frac{\mu_z(t)\theta^{z-i}}{(z-i)!} \end{cases}. \tag{4.251}$$

4.4.2 From the Chemical Master Equation to moments based descriptions

Since we will only consider the structure of the Chemical Master Equation, we would like to derive a general version of the Moment Generating Function which can be used for any system. The CME for l reactions with stoichiometric change v_l is:

$$\frac{\partial P(z,t|z_0,t_0)}{\partial t} = \sum_l a_l(z-v_l)P(z-v_l,t) - a_l(z)P(z,t). \tag{4.252}$$

As we will see later on, the kind of rate laws associated with the system dramatically impact the complexity of the overall problem. We consider the most simple case of kinetic mass action laws. An example of a mass action rate law is $a_l(z) = \frac{\lambda z_1(z_1-1)}{2} = \frac{\lambda}{2}z_1^2 - \frac{\lambda}{2}z_1 = \sum_i c_{l,i}a\prime_{l,i}$, where the law can be rewritten as a sum of coefficients $c_{l,i}$ and variables $a\prime_{l,i}$. This expanded, polynomial form will be exploited in our derivation.

Since we would like to talk about moments of the CME rather than probabilities, our first priority is to write this equation in terms of M, rather than in terms of P. We multiply both sides by $e^{\theta z}$ and sum over all possible values of z

$$\sum_{z=0}^{\infty} e^{\theta z}\frac{\partial P(z,t)}{\partial t} = \sum_{z=0}^{\infty}\sum_l e^{\theta z}a_l(z-v_l)P(z-v_l,t) - e^{\theta z}a_l(z)P(z,t), \tag{4.253}$$

that taking into account the previous definitions results

$$\frac{\partial M(\theta,t)}{\partial t} = \sum_{z=0}^{\infty}\sum_l\left(\sum_i c_{l,i}a\prime_{l,i}(z-v_l)e^{\theta z}P(z-v_l,t) - \sum_i c_{l,i}a\prime_{l,i}(z)e^{\theta z}P(z,t)\right) =$$

$$\sum_{z=0}^{\infty}\sum_l\left(\sum_i c_{l,i}a\prime_{l,i}(z-v_l)e^{\theta(z-v_l)}e^{\theta(v_l)}P(z-v_l,t) - \sum_i c_{l,i}a\prime_{l,i}(z)e^{\theta z}P(z,t)\right) =$$

$$\sum_l\left(\sum_i c_{l,i}\frac{\partial^i M}{\partial\theta^i}e^{\theta(v_l)} - \sum_i c_{l,i}\frac{\partial^i M}{\partial\theta^i}\right) = \sum_l\sum_i c_{l,i}\frac{\partial^i M}{\partial\theta^i}\left(e^{\theta(v_l)}-1\right). \tag{4.254}$$

Now, we can take the second definition of $\frac{\partial^i M}{\partial\theta^i}$ and expand $e^{\theta(v_l)}$ into its Taylor series. Notice that the summation now begins at $j=i$. When $j<i$, the index will be out of bounds and will not correspond to any physical state

$$\frac{\partial M(\theta,t)}{\partial t} = \sum_l\sum_i c_{l,i}\frac{\partial^i M}{\partial\theta^i}\left(e^{\theta(v_l)}-1\right) =$$

$$\sum_l\sum_i c_{l,i}\sum_{j=i}^{\infty}\frac{\mu_j(t)\theta^{j-i}}{(j-i)!}\left(\sum_{k=0}^{\infty}\frac{(\theta v_l)^k}{k!}-1\right). \tag{4.255}$$

Remember that the initial goal was to isolate the coefficients of θ^n in order to obtain the nth moments:

$$\frac{\partial M(\theta,t)}{\partial t} = \sum_l \sum_i c_{l,i} \sum_{j=i}^{\infty} \frac{\mu_j(t)\theta^{j-i}}{(j-i)!} \left(\sum_{k=0}^{\infty} \frac{(\theta v_l)^k}{k!} - 1 \right) =$$

$$\sum_l \sum_i c_{l,i} \left(\frac{\mu_i}{0!} + \frac{\mu_{i+1}\theta}{1!} + \frac{\mu_{i+2}\theta^2}{2!} + \cdots \right) \left(\frac{v_l\theta}{1!} + \frac{(v_l\theta)^2}{2!} + \frac{(v_l\theta)^3}{3!} + \cdots \right) =$$

$$\sum_l \sum_i c_{l,i} \left(\left[\frac{\mu_i}{0!} \frac{v_l}{1!} \right] \theta + \left[\frac{\mu_i}{0!} \frac{{v_l}^2}{2!} + \frac{\mu_{i+1}}{1!} \frac{v_l}{1!} \right] \theta^2 + \cdots \right) =$$

$$\sum_l \sum_i c_{l,i} \sum_{n=0}^{\infty} \theta^n \sum_{k=1}^{n} \mu_{i+(n-k)} \frac{1}{k!(n-k)!}. \tag{4.256}$$

Our next step will be to isolate only the coefficients of θ in order to achieve a form in which we are creating ODE's of μ rather than $M(\theta,t)$. Since $\frac{\partial M(\theta,t)}{\partial t} = \sum_n \frac{\partial \mu_n}{\partial t} \frac{1}{n!} \theta^n$, we will have to multiply both sides by $n!$ in order to isolate μ. Thus, it finally results

$$\frac{\partial \mu_n(t)}{\partial t} = \sum_l \sum_i c_{l,i} \sum_{k=1}^{n} v_l^k \mu_{i+(n-k)} \frac{n!}{k!(n-k)!}. \tag{4.257}$$

It is easy to note from the previous expression (4.257) that the equation that governs the time evolution of the moments up to a certain order implies, in general, higher order moments, and then, before solving all them, higher order moments must be written as a combination of those involved in the considered time evolution equations. These relations have in most cases an approximate character and are known as closure relations.

References

1. E. Abisset-Chavanne, R. Mezher, S. Le Corre, A. Ammar, F. Chinesta. Kinetic theory microstructure modeling in concentrated suspensions. Entropy, **15**, 2805-2832, 2013.
2. E. Abisset-Chavanne, F. Chinesta, J. Ferec, G. Ausias, R. Keunings. On the multiscale description of dilute suspensions of non-Brownian rigid clusters composed of rods. Journal of Non-Newtonian Fluid Mech., **222**, 34-44, 2015.
3. A. Ammar, F. Chinesta. A particle strategy for solving the Fokker-Planck equation governing the fibre orientation distribution in steady recirculating flows involving short fibre suspensions. In Lectures Notes on Computational Science and Engineering, Springer, **43**, 1-16, 2005.
4. A. Ammar, B. Mokdad, F. Chinesta, R. Keunings. A new family of solvers for some classes of multidimensional partial differential equations encountered in kinetic theory modeling of complex fluids. J. Non-Newtonian Fluid Mech., **139**, 153-176, 2006.
5. A. Ammar, B. Mokdad, F. Chinesta, R. Keunings. A new family of solvers for some classes of multidimensional partial differential equations encountered in kinetic theory modeling of complex fluids. Part II: transient simulation using space-time separated representations. J. Non-Newtonian Fluid Mech., **144**, 98-121, 2007.
6. A. Ammar, F. Chinesta, P. Joyot. The nanometric and micrometric scales of the structure and mechanics of materials revisited: An introduction to the challenges of fully deterministic numerical descriptions. International Journal for Multiscale Computational Engineering, **6/3**, 191-213, 2008.
7. A. Ammar, E. Cueto, F. Chinesta. Reduction of the chemical master equation for gene regulatory networks using proper generalized decompositions. International Journal for Numerical Methods in Biomedical Engineering, **28/9**, 960-973, 2012.
8. A. Ammar, M. Magnin, O. Roux, E. Cueto, F. Chinesta. Chemical master equation empirical moment closure. Biological Systems, **5/1**, 1000155, 2016.
9. H. Ben Dhia. Multiscale mechanical problems: the Arlequin method. C. R. Acad. Sci., 899-904, 1998.
10. B. A. Bernevig, D. Giuliano, R. B. Laughlin. Coordinate representation of the one-spinon one-holon wavefunction and spinon-holon interaction. Phys. Rev. B, **65**, 195112, 2002.
11. J.L. Basdevant. 12 Leçons de mcanique quantique. Vuibert, 2006.
12. C. Binetruy, F. Chinesta, R. Keunings. Flows in polymers, reinforced polymers and composites. A multiscale approach. Springerbriefs, Springer, 2015.
13. R.B. Bird, C.F. Curtiss, R.C. Armstrong, O. Hassager, in Dynamic of Polymeric Liquids. Wiley, New York, 1987.
14. E. Cancès, M. Defranceschi, W. Kutzelnigg, C. Le Bris, Y. Maday, Computational quantum chemistry: a primer. Handbook of Numerical Analysis, Vol. X, Elsevier, 3-270, 2003.
15. C.V. Chaubal, A. Srinivasan, O. Egecioglu, L.G. Leal. Smoothed particle hydrodynamics techniques for the solution of kinetic theory problems. J. Non-Newtonian Fluid Mech., **70**, 125-154, 1997.
16. F. Chinesta, G. Chaidron, A. Poitou. On the solution of the Fokker-Planck equation in steady recirculating flows involving short fibre suspensions. J. Non-Newtonian Fluid Mech., **113**, 97-125, 2003.
17. F. Chinesta, A. Ammar, A. Falco, M. Laso. On the reduction of stochastic kinetic theory models of complex fluids. Modeling and Simulation in Materials Science and Engineering, **15**, 639-652, 2007.
18. F. Chinesta, M. Mackley, Microstructure evolution during liquid-liquid laminar mixing: A kinetic theory approach. International Journal of Material Forming, **1**, 47-55, 2008.
19. F. Chinesta, A. Ammar, A. Leygue, R. Keunings. An overview of the Proper Generalized Decomposition with applications in computational rheology. Journal of Non Newtonian Fluid Mech., **166**, 578-592, 2011.
20. F. Chinesta, R. Keunings, A. Leygue. The Proper Generalized Decomposition for Advanced Numerical Simulations: A Primer. SpringerBriefs in Applied Science and Technology.

21. F. Chinesta, E. Abisset, A. Ammar, E. Cueto. Efficient numerical solution of continuous mesoscale models of complex fluids involving the Boltzmann and Fokker-Planck quations. Communications in Computational Physics, **17/4**, 975 -1006, 2015.
22. D.B. Cook, Handbook of computational chemistry. Oxford University Press, 1998.
23. P.G. de Gennes. Repation of a polymer chain in the presence of fixed obstacles. The Journal of Chemical Physics, **55/2**, 572-579, 1971.
24. B. Diu. Trait de physique lusage des profanes. Odile Jacob, 2000.
25. M. Doi, S.F. Edwards. Dynamics of rod-like macromolecules in concentrated solution. J. Chem. Soc., Faraday Trans., **74**, 560-570, 1978.
26. M. Doi, S.F. Edwards, The Theory of Polymer Dynamics. Clarendon Press, Oxford, 1987.
27. M. Doi, T. Ohta, Dynamics and rheology of complex interfaces. J. Chem. Phys., **95**,1242-1248, 1991.
28. J. Donea, A. Huerta. Finite Element Methods for Flow Problems. Wiley, 2003.
29. P. Español, P. Warren. Statistical mechanics of Dissipative Particle Dynamics. Europhys. Lett., **30/4**, 191-196, 1995.
30. J. Gribbin, In Search of Schrdingers cat. Bantam Books, 1984.
31. Handbook of Numerical Analysis, Vol. X: Computational Chemistry, C. Le Bris editor, Elsevier, 2003.
32. J. Hladik. Pour comprendre simplement les origines de lvolution de la Physique quantique. Ellipses, 2007.
33. A. Jaishankar, G. McKinley. Power-law rheology in the bulk and at the interface: quasi-properties and fractional constitutive equations. Proc R Soc. A, **469**, 20120284, 2012.
34. G.B. Jeffery. The motion of ellipsoidal particles immersed in a viscous fluid. Proc. R. Soc. Lond., **A102**, 161-179, 1922.
35. O. Koch, W. Kreuzer, A. Scrinzi. Approximation of the time-dependent electronic Schrödinger equation by MCTDHF. Applied Mathematics and Computation, **173**, 960-976, 2006.
36. A. Kilbas, H.M. Srivastava, J.J. Trujillo. Theory and applications of fractional differential equations, Elsevier, 2006.
37. J. Klafter, A. Blumen, M. F. Shlesinger. Stochastic pathway to anomalous diffusion. Physical Review A, **35/7**, 3081-3085, 1987.
38. R.B. Laughlin, The theory of everything, Proceeding of the U.S.A. National Academy of Sciences, 2000.
39. A. Ma, F. Chinesta, A. Ammar, M. Mackley. Rheological modelling of Carbon Nanotube aggregate suspensions. Journal of Rheology, **52/6**, 1311-1330, 2008.
40. A. Ma, F. Chinesta, M. Mackley. The rheology and modelling of chemically treated Carbon Nanotube suspensions. Journal of Rheology, **53/3**, 547-573, 2009.
41. R. Omnès. Les indispensables de la mcanique quantique. Odile Jacob, 2006.
42. S. Ortoli, J.P. Pharabod. Le cantique des quantiques. La Dcouverte, 1984
43. H.C. Ottinger. Stochastic Processes in Polymeric Fluids. Springer, Berlin, 1996.
44. I. Podlubny. Fractional differential equations, Academic Press, San Diego, 1999.
45. A. Rae. Quantum Physics: Illusion or Reality?. Cambridge University Press, 2004.
46. E. Schrödinger. What is life? The physical aspect of the living cell, Dublin Institute for Advanced Studies at Trinity College, Dublin, 1944.
47. V.B. Shenoy, R. Millera, E.B. Tadmor, D. Rodney, R. Phillips, M. Ortiz. An adaptive finite element approach to atomic-scale mechanics – the quasicontinuum method. Journal of the Mechanics and Physics of Solids, **36**, 500-531, 1999.
48. S. Succi. The Lattice Boltzmann equation for fluid dynamics and beyond. Clarendon Press, Oxford, 2001.
49. R. Tanner. Engineering Rheology. Oxford University Press, 1985.
50. G.J. Wagner, W.K. Liu. Coupling of atomistic and continuum simulations using a bridging scale decomposition. Journal of Computational Physics, **190**, 249-274, 2003.
51. J.H. Weiner, Statistical mechanics of elasticity. Dover, 2002

References

52. E.D. Wetzel, C.L. Tucker III. Area tensors for modeling microstructure during laminar liquid-liquid mixing. International Journal of Multiphase Flow, **25**, 35-61, 1999.
53. E. Wichmann. Quantum Physics. McGraw-Hill, 1971.
54. S.P. Xiao, T. Belytschko. A bridging domain method for coupling continua with molecular dynamics. Comput. Methods Appl. Mech. Engrg., **193**, 1645-1669, 2004.